Parallel and converging multisensory cascades in the *Drosophila* connectome

Richard Betzel[1,2],* Maria Grazia Puxeddu[3], Caio Seguin[4], and Bratislav Misic[5]
[1]*Department of Neuroscience, University of Minnesota, Minneapolis MN 55419*
[2]*Masonic Institute for the Developing Brain, University of Minnesota, Minneapolis MN 55413*
[3]*Department of Computer, Control, and Management Engineering, University of Rome La Sapienza, Rome, Italy*
[4]*Department of Psychiatry, The University of Melbourne, Melbourne, VIC, Australia and*
[5]*McConnell Brain Imaging Centre, Montréal Neurological Institute, McGill University, Montréal, Canada*
(Dated: December 2, 2024)

Connectomes are network maps of synaptic connectivity. A key functional role of any connectome is to constrain inter-neuronal signaling and to sculpt the flow of activity across the nervous system. Connectomes therefore play a central role in the rapid tranmission of information about an organism's environment from sensory neurons to higher-order neurons for action planning and ultimately to effectors. Here, we use a parsimonious model of activity spread to investigate the connectome's role in shaping putative sensory cascades. Our model allows us to simulate the signaling pathways from sensors to the rest of brain, mapping the similarity of these pathways between different sensory modalities and identifying convergence zones–neurons that are activated simultaneously by different sensory modalities. Further, we considered two multisensory integration scenarios – a cooperative case where different sensory modalities interacted to "speed up" (reduce) neurons' activation times and a competitive "winner take all" case, where different sensory streams vied for the same neural territory. Finally, we use a data-driven algorithm to partition neurons into different classes based on their behavior during the cascade simulations. Our work helps underscore the role of "simple" models for enriching connectome data, while offering a data-driven classification of neurons based on their joint connectional/dynamical properties.

INTRODUCTION

Connectomes are wiring maps that describe the interconnectivity of neural elements–cells, populations, areas–to one another [1–6]. These physical connections facilitate communication and signaling between neural elements [7–10]. The structure of the connectome allows transduced sensory information from an organism's environment to be transmitted to and processed by other neural elements, helping to coordinate contextually appropriate and adaptive behavioral responses to environmental stimuli [11–14]. Discovering and modulating the pathways that shape the flow of sensory information is a key aim of systems and behavioral neuroscience [15, 16].

Network neuroscience is the nascent discipline associated with mapping and analyzing brain network data [15]. In this framework, connectomes of neural elements and their pairwise connections are represented as networks (graphs) of nodes and edges and encoded in adjacency/connectivity matrices [17]. The structure of these networks can be described directly using analytic tools from graph theory [18–25], but can also serve to constrain simulations of brain dynamics [26–30].

Indeed, network neuroscience provides useful frameworks for studying dynamic flows over a network. For instance, spreading models imagine a set of initially active nodes ("seeds") that in subsequent time steps "infect" or activate their downstream neighbors [31–34]. For certain sets of parameters, these models give rise to "cascades," wherein the seeds activate their neighbors, who later activate *their* neighbors, who in turn activate *their* neighbors, and so on, until the majority of nodes in the network have been activated. These types of models represent an analytically tractable framework for studying the interplay of network structure with dynamics. Moreover, spreading models can be viewed as idealized models of sensory cascades [35], tracking the timing of activations from an initially active population of sensory neurons (activated directly by the sensory stimulus), through the nervous system, and eventually to effectors [36].

Recently, there has been a concerted effort to map connectomes with varying levels of completeness for a select set of organisms at the nano-scale–i.e. single-neuron, single-synapse resolution [9, 37–46]. The resulting connectome maps afford network neuroscience researchers the opportunity to probe network structure with unprecedented granularity. Presently, the largest complete connectome is that of a single adult female fruit fly – *Drosophila melanogaster* [47]. It is composed of approximately 134,000 neurons, 15 million binary connections, and 54 million synapses. Importantly, the neurons and synapses of this connectome have also been expertly annotated [48–50], making it possible to augment the results of network neuroscientific analyses with links to cells putative type, function, and lineage [51].

The annotation data also distinguishes sensory neurons from the rest of the brain and further subdivides these neurons into distinct sensory modalities.

* Correspondence email address: rbetzel@umn.edu

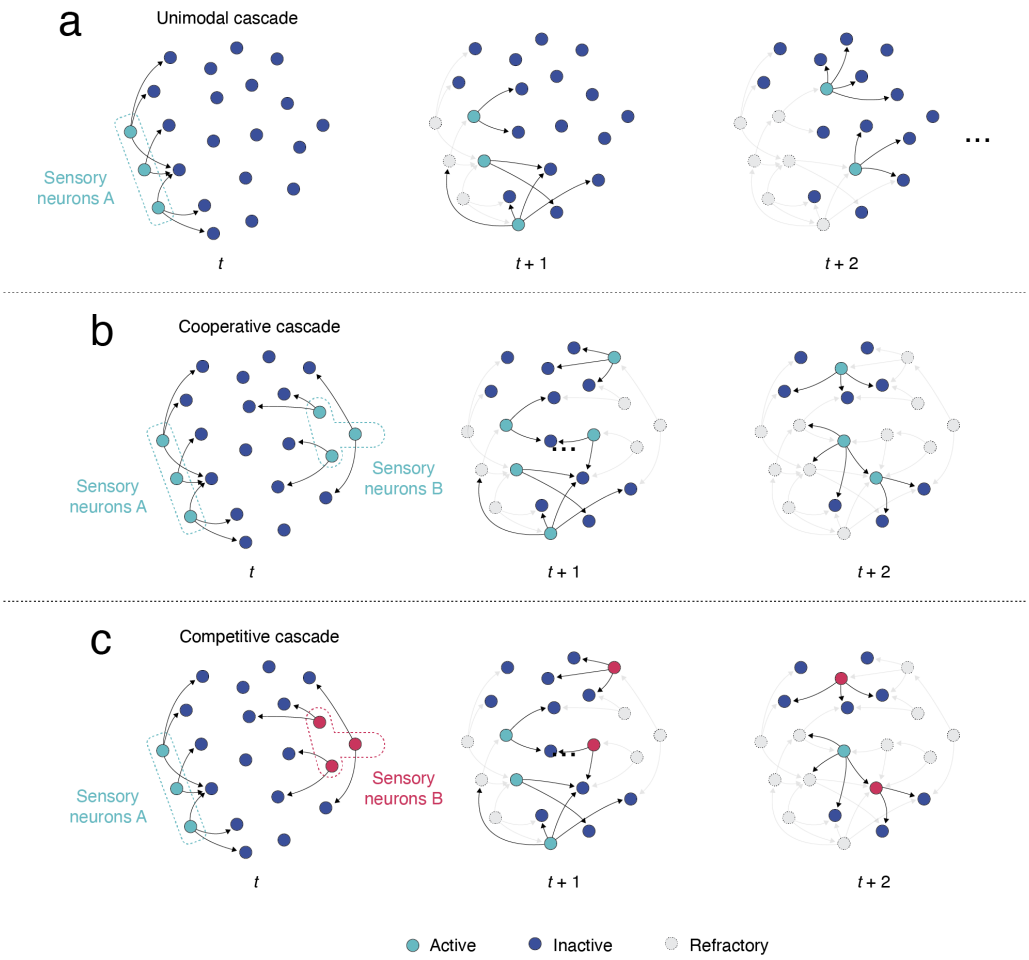

Figure 1. **Schematic illustration of cascade model.** Neurons can take on three states; active, inactive, or refractory. Inactive neurons are activated probabilistically by their pre-synaptic partners. Once a neuron has been activated, it enters a refractory period, wherein it cannot be activated at any subsequent time point. We consider three variations of this model. (*a*) Unimodal sensory cascades: wherein the initial population of active neurons (the seed population) are all of the same sensory modality. The model proceeds until either all neurons have been activated or there exists a time point wherein no neurons are currently active. (*b*) Cooperative sensory cascades: we consider two populations of sensory neurons, each of which represents a different sensory modality. Nonetheless, in their active states, these neurons carry identical information (the same state value), and therefore generally improve (reduce) activation times such that neuron i will tend to be activated earlier in the cooperative condition than in the unimodal condition. (*c*) Competitive sensory cascades: we, again, consider two populations of sensory neurons, but force them to carry different information and therefore "compete" for territory.

These annotations make it possible to seed, in a cascade model, specific populations of sensory neurons and tracking the spread of activation through the network. With this type of model, we can address the following questions: How do sensory signals propagate through the *Drosophila* brain? How quickly do the signals spread? Which synaptic connections ensure rapid transmission? Where in the brain do multisensory signals converge? *When* does this convergence take place? Which architectural features support multisensory integration?

Here, we perform precisely these types of analyses. Specifically, we apply a recently developed spreading model [52] to explore three scenarios: (*1*) unimodal cascades, wherein cascades are initiated from distinct sensory systems independently (Fig. 1a); (*2*) cooperative cascades, wherein cascades are initiated in pairs of sensory systems to synergistically reduce (or maintain) the activation times of downstream neurons (Fig. 1b); and (*3*) competitive cascades, where, once again, cascades

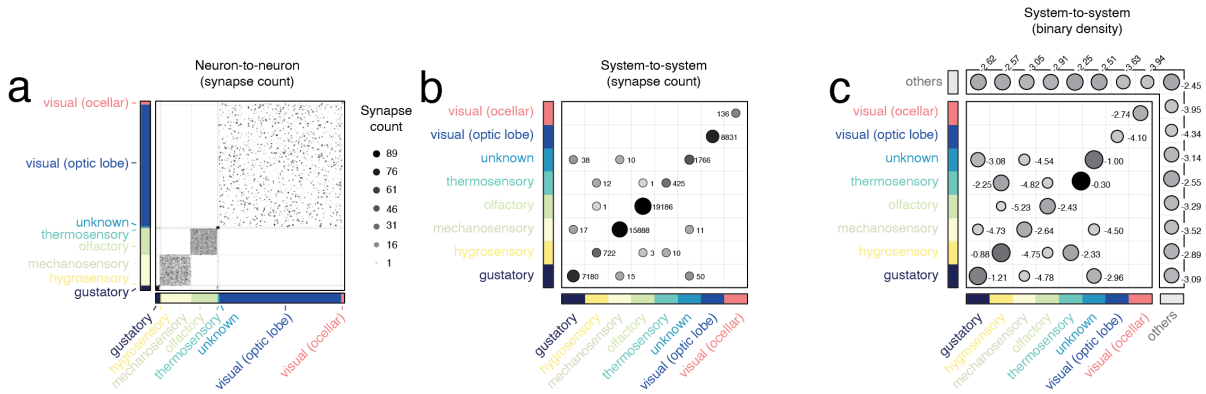

Figure 2. **Synaptic connectivity within and between primary sensory neurons.** (a) Complete sub-network of sensory-to-sensory connections. Gray lines delineate systems (modalities) from one another. (b) Synapse count between pairs of systems. (c) Binary density of connections between pairs of systems (and remaining neurons, labeled "others"). Note that in c the color and labels are on a logarithmic scale.

are initiated in pairs of sensory systems, but where the signals competitively interact, vying for territory with one another (Fig. 1c). We show that initially sensory systems follow distinct trajectories–i.e. probabilistic maps of when neurons are active–yet converge onto a relatively small set of higher-order neurons in the central complex. Further, we map the set of neurons and their synaptic connections that facilitate the early spread of activation through the fly brain. Next, consider the cooperative scenario and find only marginal reductions in activation time. Next, we explore the competitive cascade scenario and identify groups of neurons that sit at the boundary between the territories traced out by the competing sensory cascades. Finally, to identify groups of neurons that play similar roles in the context of the spreading model, we use a data-driven approach to partition neurons based on a series of cascade-derived summary statistics.

RESULTS

Here we analyzed the connectome of a single adult female*Drosophila melanogaster* (publicly available through `https://codex.flywire.ai/`; all analyses were carried out on the v783 connectome) [47]. The connectome comprised $N = 138,639$ neurons, $M = 15,091,983$ edges, $M_w = 54,492,922$ synapses.

Neuronal wiring of sensory systems

Synaptic connectivity between pairs of neurons allow signals–including sensory information–to propagate throughout a nervous system. The configuration of connections among neurons–the connectome's topology–therefore plays an important role in sculpting information flows [53]. Here, in order to investigate the role of network structure in sensory integration, we focus first on the wiring within and between $N_{sensory} = 16,349$ sensory neurons, each of which represent distinct sensory modalities: gustation, hygrosensation, mechanosensation, olfaction, thermosensation, vision–optic lobe and ocellar–and an "unknown" class of sensory neurons.

Specifically, we extracted the 16349×16349 dimensional subgraph of all synaptic connections between pairs of sensory neurons (Fig. 2a). This subgraph was particularly sparse (a binary density of $d_{sensory} = 1.3 \times 10^{-4}$). In comparison, the density of the whole-brain connectome is $d_{connectome} = 7.8 \times 10^{-4}$ (approximately six times denser). Indeed, the sensory subgraph is significantly sparser than randomly-sampled subgraphs of equal size ($p < 10^{-3}$; 1000 random samples).

The subgraph of sensory neurons is also extremely modular, which is immediately evident upon visual inspection (Fig. 2a). Of all synapses in the subgraph, 99.7% (54134 out of 54302) occur between pairs of neurons associated with the same sensory modality (Fig. 2b).

The direct wiring of sensory neurons to one another is therefore largely parallel and modular; that is, there exists near-minimal cross-connectivity between sensory modalities. Given this level of sparseness, these observations suggest that integration of multi-modal sensory signals likely requires poly-synaptic and extra-sensory pathways. We explore the combined role of direct and

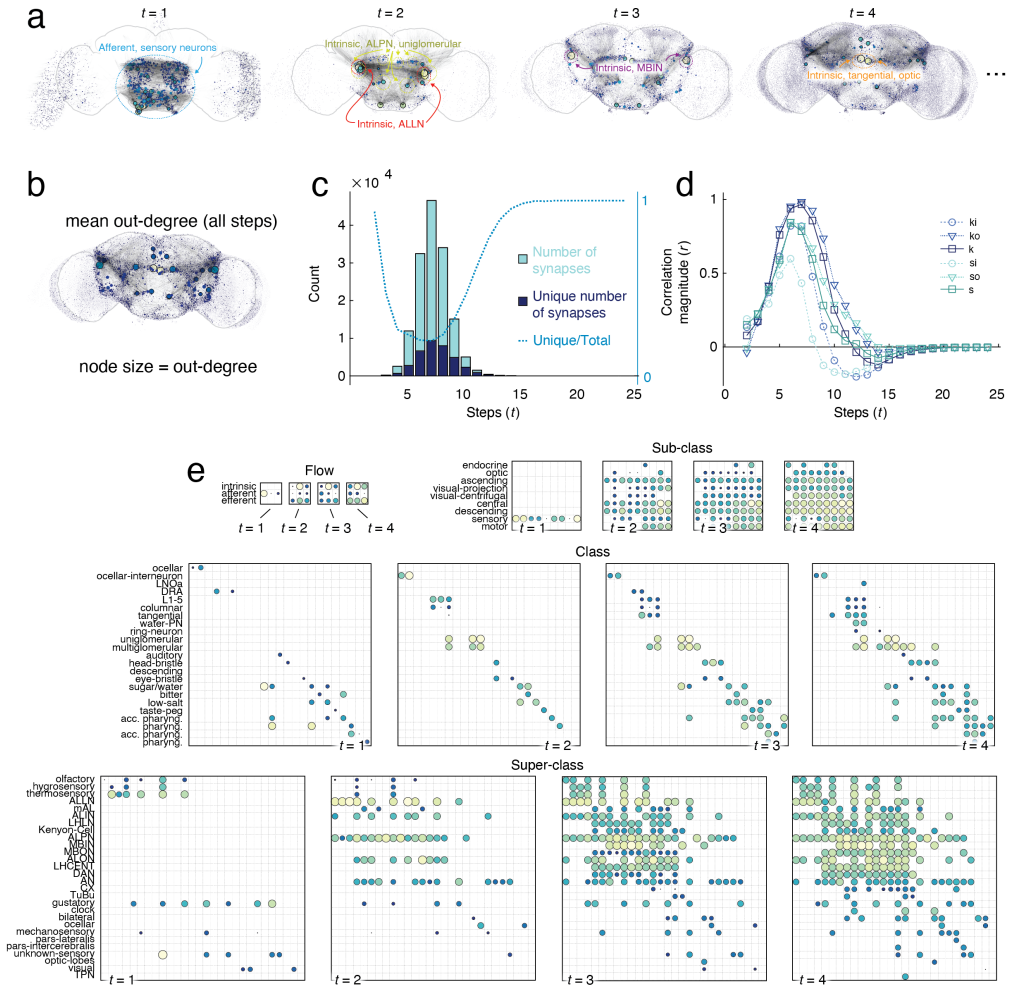

Figure 3. **Edge sequencing.** (a) Top 1000 edges (by usage) over first four time steps. (b) We constructed a weighted connectivity matrix by averaging edge usage across all time points, where at each time point an edge is present if it activates a postsynaptic neuron. We then calculate the out-degree of each node to highlight influential spreaders. (c) Across 1000 simulations, we count the total number of active synapses at each time point along with the unique number of active synapses. If the same synapses were active across all runs, then these numbers would coincide; however, due to the stochasticity of the cascade model and variation in the set of seeded neurons, different synapses appear at different time points. (d) Correlation of the instantaneous out-degree with basic structural properties of the network. (e) Active synapses (edges) grouped by annotation data. Circumference and color circle are proportional to the logarithm of their usage (count).

indirect pathways in the subsequent sections using a stylized *cascade model* to investigate the spatiotemporal trajectory of activation spreading following synaptic signaling events. Note that in all subsequent sections, we expand our analyses from the sensory subgraph described here, to the entire connectome.

The model we study is stochastic and abstract. In principle, it is applicable to any networked system [54]. Neurons can take on one of three states: active, inactive, or quiescent. Initially (at time $t = 0$), a small set of N_{seed} "seed" neurons are considered "active"; all other neurons are "inactive". We can think of the seed neurons as those activated directly by a sensory stimulus. At the following time step, previously-active neurons activate their post-synaptic partners with probability, $p_{transmission}$. In parallel, the previously-active neurons become "quiescent," and cannot be activated again. This sequence continues until every neuron is either inactive or quiescent, at which point the simulation ends. See Fig. S1 for example cascades and for more details on the dependence of cascade properties on parameter values.

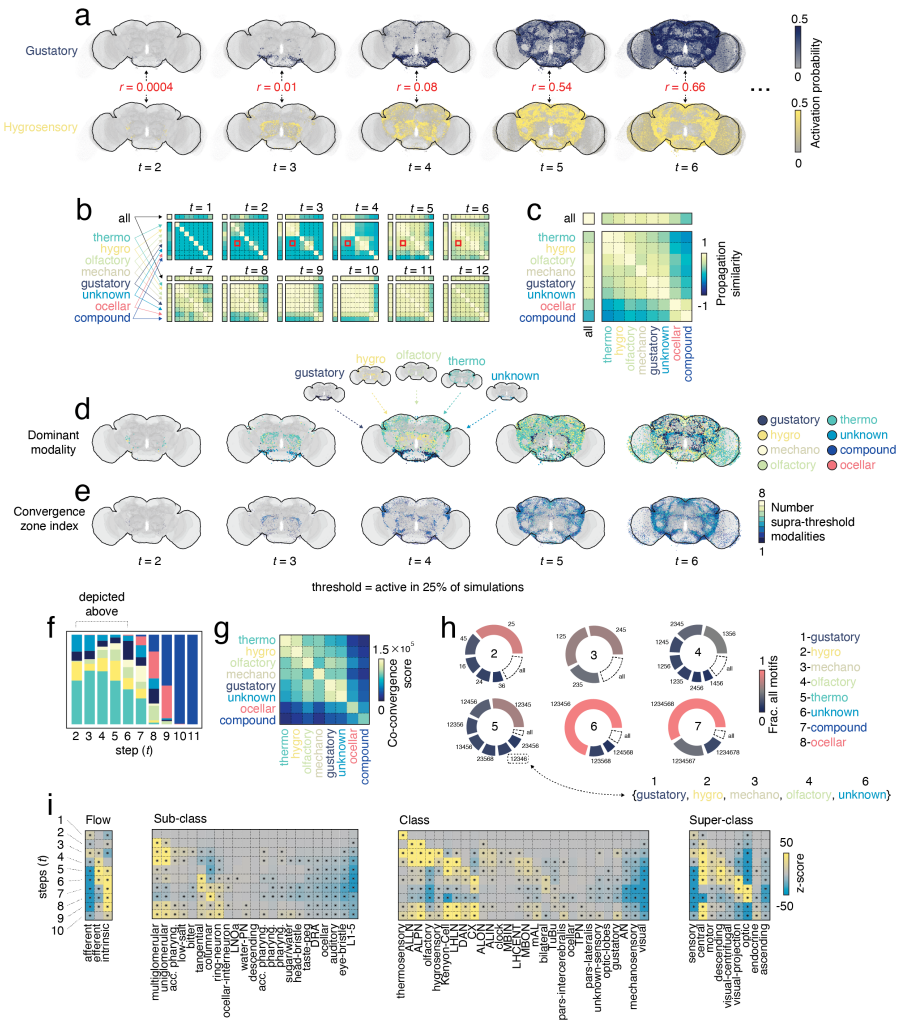

Figure 4. **Modal specificity and similarity of cascades.** Here, we consider cascades in which neurons associated with different sensory modalities are treated as seeds. From these seeds we simulate cascades and compare the spatiotemporal trajectories between sensory modalities. (a) Schematic for comparing cascades. For two sensory modalities (gustation and hygrosensation, in this case) we calculated the similarity between spatial maps at each time step as a correlation. (b) We extended this comparison to all pairs of sensory modalities as well as the "all" category (pan-sensory cascade), wherein sensory neurons from all modalities are treated as seeds, and show the similarity between all pairs at each time step, from $t = 1$ to $t = 12$. (c) We also concatenated the activation probability maps across time steps for a given sensory modality and computed the similarity between these omnibus maps, yielding a single time-invariant similarity score for pairs of sensory modalities. (d) We calculated dominance maps, where each neuron is assigned the label of the sensory modality corresponding to the greatest activation probability at a given time step. (e) We also calculated a "convergence index" for neurons as the number of sensory modalities with activation probability exceeding some threshold (here, 25%) at a given time step. (f) Composition of dominant modality as a function of time. (g) Pairwise co-convergence between pairs of sensory modalities. That is, how often did two sensory modalities simultaneously exceed the activation probability threshold together. (h) Frequency of overlap motifs, ranging from size 2 to size 7. (i) Enrichment statistics for convergence zone index across annotations as a function of time.

Edge contributions to cascades

Sensory cascades are facilitated by the sustained and mass activation of post-synaptic neurons by their pre-synaptic partners. One particularly interesting feature of the spreading model is its ability to track the specific (sets of) synapses through which those activations spread, thereby allowing us to identify putative sensory pathways – sequences of synaptic contacts ("edges") –

that support sensory cascades. We can then ask what types of neurons preferentially participate in these pathways? How does the network of active synapses relate to the underlying connectome topology? Are neurons with many active synapses also connectome hubs?

To address these kinds of questions, we first calculated three quantities of interest: the total number of active synapses at each time step, the total number of unique synapses active at that time step, and the ratio of those two measures (unique/total). If the same set of synapses were active across successive runs, then the ratio would approach 1. However, if every run utilized non-overlapping sets of synapses, then the ratio would approach 0. Note that here, we focus on a scenario in which the set of initially active seed neurons was randomly and uniformly sampled from across all sensory neurons (all modalities). We describe results with the $N_{seed} = 16$ and $p_{transmission} = 0.01$.

We found evidence of a "bottlenecking" effect, wherein the same synapses were consistently used to propagate activity from the seeded sensory neurons to the rest of the *Drosophila* brain (Fig. 3a). Following this period of high consistency, the ratio of unique to total active synapses dropped rapidly, suggesting that there exists a plurality of secondary pathways that allow cascades to propagate beyond sensory neurons. This reduction continues until it achieves a local minimum before a slower return to unity (Fig. 3c).

How are synapse activation patterns related to connectome wiring? Can we determine in advance, and based only on the direct connections encoded in the connectome, which synapses are critical for igniting and/or perpetuating signaling cascades? To address this question, we calculated neurons' out-degrees at each time step based on the edge usage (synapse activation) map and compared these values to neurons' in/out/total degrees and strengths, as derived from the connectome. We found that, initially, the correlation is low (maximum $r = 0.15$), suggesting that the initial propagation step is not driven by hub nodes–those with many outgoing connections–in the complete connectome (Fig. 3d). However, as the cascade evolves, the correspondence between edge usage and connectome degree increases, reaching a magnitude $r > 0.9$ by $t = 7$ and reflecting the increased dependence on hub neurons for perpetuating later stages of the cascade.

In addition, we used annotation data to better contextualize and understand edge usage maps. Specifically, we aggregated the elements of the edge usage matrix at each time step (a $[138,639 \times 138,639]$ matrix) by annotation categories –"Flow", "Super-class", "Class", and "Sub-class" (Fig. 3e; see **Materials and Methods** for details on annotations). We find that the early stages of cascades are driven by synapses between afferent and intrinsic neurons (Fig. 3e, top left). These afferent neurons were, as expected, largely sensory neurons (Fig. 3e, top right). We also find evidence that uni-/multi-glomerular neurons are critical for propagating cascades at secondary and tertiary stages (Fig. 3e,middle) *via* reciprocal connections to their uni-/multi-glomerular neurons as well as tangential neurons. Similarly, antennal lobe (ALON, ALPN, ALIN, ALLN) along with mushroom body neurons (including Kenyon cells) play critical roles in the activation of postsynaptic partners from timestep $t = 2$ and beyond (Fig. 3e,bottom). Specifically, these neurons project to other neurons in the central complex, leading to their activation at subsequent timesteps, before ultimately activating neurons in the optic lobes.

Overlapping and distinct spatiotemporal profiles of unimodal sensory cascades

In the previous section we introduced the cascade model and plotted summary statistics for simulations in which neurons associated with *all* sensory systems were included in the set of initially active seed neurons. Here, we separately seed each of the eight sensory modalities, parsing out the shared and unique features of modality-specific cascades.

To highlight unique and dissimilar features of sensory cascade, we show activation probabilities from time steps $t = 2$ to $t = 6$ for gustatory and hygrosensory seeds (Fig. 4a). The activation probability maps begin effectively uncorrelated, which reflects the largely non-overlapping wiring of the two sensory systems. However, as the cascade evolves, the activation probability maps increase their similarity to one another.

This pattern of behavior is common when comparing sensory cascades to one another. Although sensory systems are distinct from one another at early time points, we find that they coalesce into larger clusters before forming becoming uniformly similar to one another (Fig. 4b). Specifically, we find that thermosensory, hygrosensory, and olfactory cascades exhibit similar activation probability maps beginning at step $t = 2$ and persisting as a differentiable cluster until around $t = 5$. Similarly, gustatory and "unknown" sensory neurons form a small cluster beginning at $t = 3$ before incorporating mechanosensory neurons at $t = 4$. The most distinct cascades originate with ocellar and compound visual neuron. They remain dissimilar to virtually all other sensory systems until $t = 6$, form a small cluster themselves beginning at $t = 7$, and remain largely distinct through, at least, $t = 12$. We also summarize these relationships more succinctly by computing an "omnibus" similarity matrix. Specifically, for each sensory modality, we concatenate the activity probability maps from $t = 1$ through $t = 12$ into a single vector of length $N_{neurons} \times 12$. We then compare sensory modalities to one another by computing

the correlation of these concatenated maps (Fig. 4c). Note that, broadly, this pattern recapitulates the underlying anatomical connectivity. That is, sensory modalities with similar connectivity patterns tend to exhibit greater similarity in terms of their cascades (Fig. S2).

To further compare sensory modalities, we calculated two complementary statistics. For each neuron, i, we estimated its "dominant" sensory modality–i.e. the sensory modality corresponding to that neuron's maximum activation probability–at every time step (Fig. 4d). However, this "winner-take-all" approach can be misleading; the dominant modality may exceed the next-greatest activation probability by an arbitrarily small amount. Accordingly, we also calculated a second related statistic, which we refer to as the "convergence zone index." This metric calculates the number of unimodal sensory cascades with activation probability greater than a user-defined threshold–set here to 25%–at time t (Fig. 4e).

Interestingly, we find that the composition of dominant modalities is not fixed across time. From time steps $t = 2$ to $t = 6$, thermosensory neurons are the clear winner, dominating more than 50% of all neurons at $t = 4$, suggesting that the wiring of thermosensory neurons may facilitate rapid signal propagation. This dominance crescendos at steps $t = 3$ and $t = 4$ before beginning a gradual decline. This decline corresponds to the increased dominance of hygrosensory, olfactory, mechanosensory, and gustatory cascades over steps $t = 3$ to $t = 7$. Conspicuously absent in these early stages are visual cascades (ocellar and compound visual neurons), which only begin to acquire territory around $t = 7$ and persisting until $t = 11$. During this time period, the cascades of other sensory modalities have already reached their peaks and have begun to terminate.

We also derived summary statistics from the convergence zone measure. For instance, we can count how often sensory cascades co-converge upon the same sets of neurons. Consider, for example, hygrosensory and gustatory cascades. We counted, for any given neuron, the number of time points for which that neuron's activation probability was supra-threshold for both hygrosensory *and* gustatory cascades (its co-convergence score). We did the same for all neurons and all time points, and calculated their sum to obtain a total co-convergence score for every pair of sensory systems. The structure of the co-convergence matrix (Fig. 4g) largely mirrors the cascade similarity matrix–visual cascades generally do not co-converge onto the same neurons as the other sensory systems and, among those systems, there is clear cluster structure, with thermosensory + hygrosensory and gustatory+unknown cascades co-converging on similar neurons. Here, however, we find evidence supporting the uniqueness of mechanosensory and olfactory cascades, with neither exhibiting clear correspondence to either cluster.

Next, we investigated the pairings of systems with one another. That is, when two sensory cascades converge onto the same neuron, which pairing occur most frequently? When a triplet, quartet, quintet, etc. of cascades converge on a neuron, what is the composition of those groups? Here, we report the most frequent compositions for groups of size 2 to 7: hygrosensory + thermosensory; hygrosensory + oflactory + thermosensory; gustatory + mechanosensory + olfactory + unknown; gustatory + hygrosensory + mechanosensory + olfactory + thermosensory; gustatory + hygrosensory + mechanosensory + olfactory + thermosensory + unknown; and gustatory + hygrosensory + mechanosensory + olfactory + thermosensory + ocellar (Fig. 4h). For the parameter values reported here, we never observed any neurons onto which all eight sensory cascades converged.

Finally, we performed a time-varying enrichment analysis of the convergence zone statistic. At each time, t, we calculated the mean convergence score for every annotation and standardized these scores (z-scored) against a null distribution estimated by randomly permuting annotation labels (Fig. 4i). In the first step, afferent (flow), thermosensory (class), and sensory (superclass) neurons are highly enriched for convergence. This is consistent with the seeding procedure. At the next step, we find that multi-/uni-glomerular (sub-class), antennal lobe (input, projection, output; class), and central neurons (super-class) are all enriched. This findings aligns with the previous observation that edges incident upon those categories of neurons were critical for propagating cascades beyond the initial step. As the cascade progresses, different annotations become convergence-enriched. For instance, efferent and intrinsic neurons become strongly enriched between steps 3 and 4 and step 5, respectively (flow); tangential and columnar neurons become enriched at steps 6 and 7 (sub-class); Kenyon cells and lateral horn neurons are enriched at step 4 (class), followed by central complex neurons (step 6); central neurons, motor, descending, visual centrifugal and projection, and optic neurons, all are enriched between steps 3 through 8.

Collectively, these results suggest that sensory cascades are initially propagated through largely non-overlapping but highly consistent pathways to secondary sets of neurons. These secondary sets, which are broader, are composed largely of intrinsic neurons situated in the central brain. Sensory cascades originating in visual neurons (compound and ocellar) are outliers, and are comparatively distinct in terms of their trajectories.

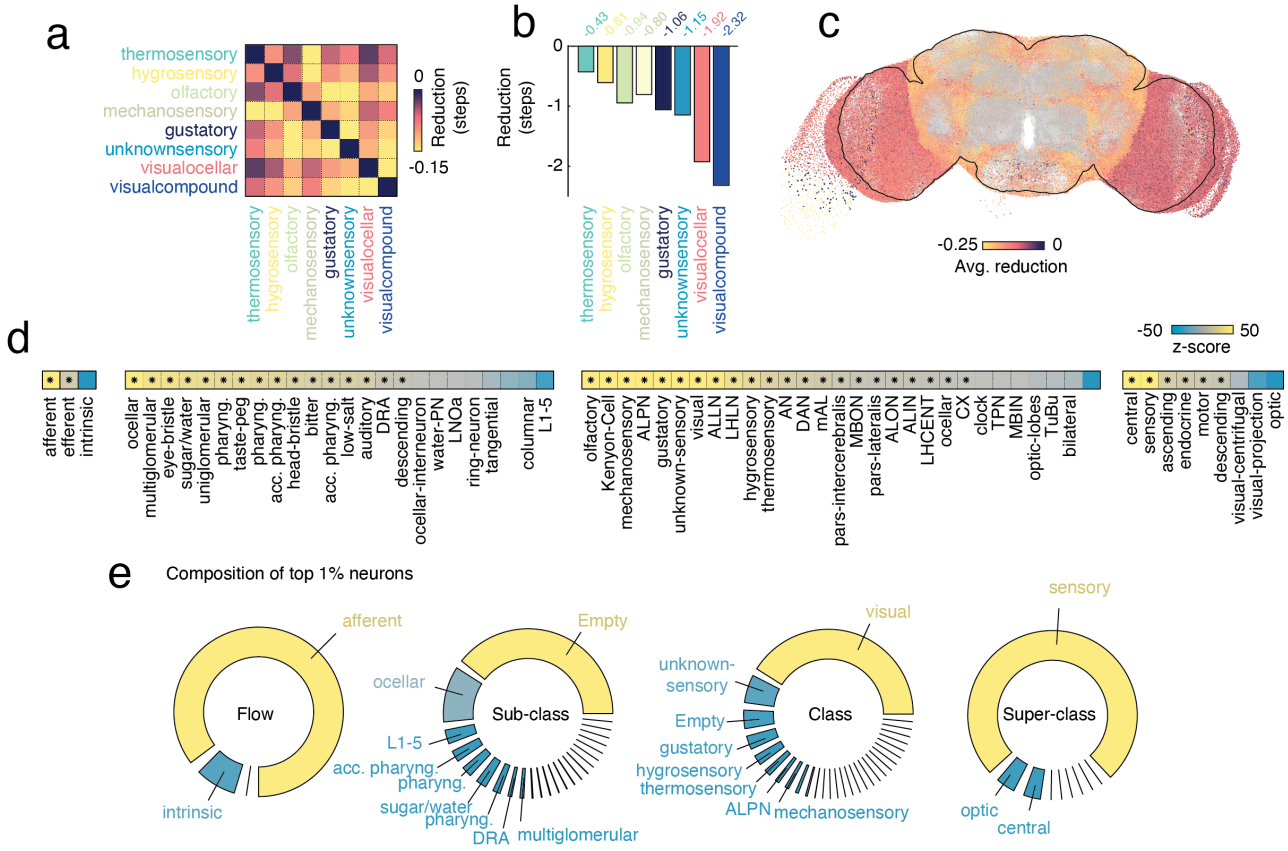

Figure 5. **Cooperative cascade statistics.** Here, we consider cascades in which neurons associated with different sensory modalities are treated as seeds. In contrast with the competitive cascade model, where postsynaptic neurons are activated by one sensory modality or the other, neurons here can be activated by *either* sensory modality. In principle, then, the cooperative cascade leads to reductions in activation time for "synergistic" sensory modalities. That is, pairs that target distinct neuronal populations or sufficiently enhance the probability of activating a single neuronal population. (*a*) Average reduction in activation time for all pairs of sensory modalities. Note that the colormap is inverted, so that the greatest reductions are depicted in bright colors. (*b*) We also compared unimodal cascade activation times against the scenario where *all* neurons in all sensory modalities are seeded. Here, we show the mean reduction in activation time for such a scenario. (*c*) The same information at single-cell resolution and in anatomical space. (*d*) Enrichment statistics for speed-ups. (*e*) The distribution of speed-ups was heavy-tailed. Here, we highlight the tail of this distribution (the top 1% of neurons by average reduction in activation time), showing their composition across annotation categories.

Cooperative sensory cascades

At the end of the previous section, we defined a measure–the convergence zone–to relate the spatiotemporal trajectories of multiple sensory cascades to one another. However, the convergence zone is calculated based on non-interacting cascades. A slightly more realistic extension of the cascade model is to allow for cascades to interact with one another, either cooperatively or competitively. Here, and in the following subsection, we consider interacting sensory cascades, beginning with a "cooperative" model in which the seed list includes neurons from pairs of sensory modalities–e.g. hygrosensory seeds *and* thermosensory seeds. Postsynaptic neurons can be activated by either of the two seeds. Consequently, neurons will generally reduce their activation time under a cooperative cascade. Intuitively, we can think of a cooperative cascade in terms of polysensory integration–e.g. a change in visual field that occurs simultaneously with a change in temperature. By pairing these stimuli together, we increase the likelihood and speed by which that sensory information is propagated through the nervous system. In this section, we characterize properties of cooperative cascades.

As a first test, we simulated polysensory cooperative

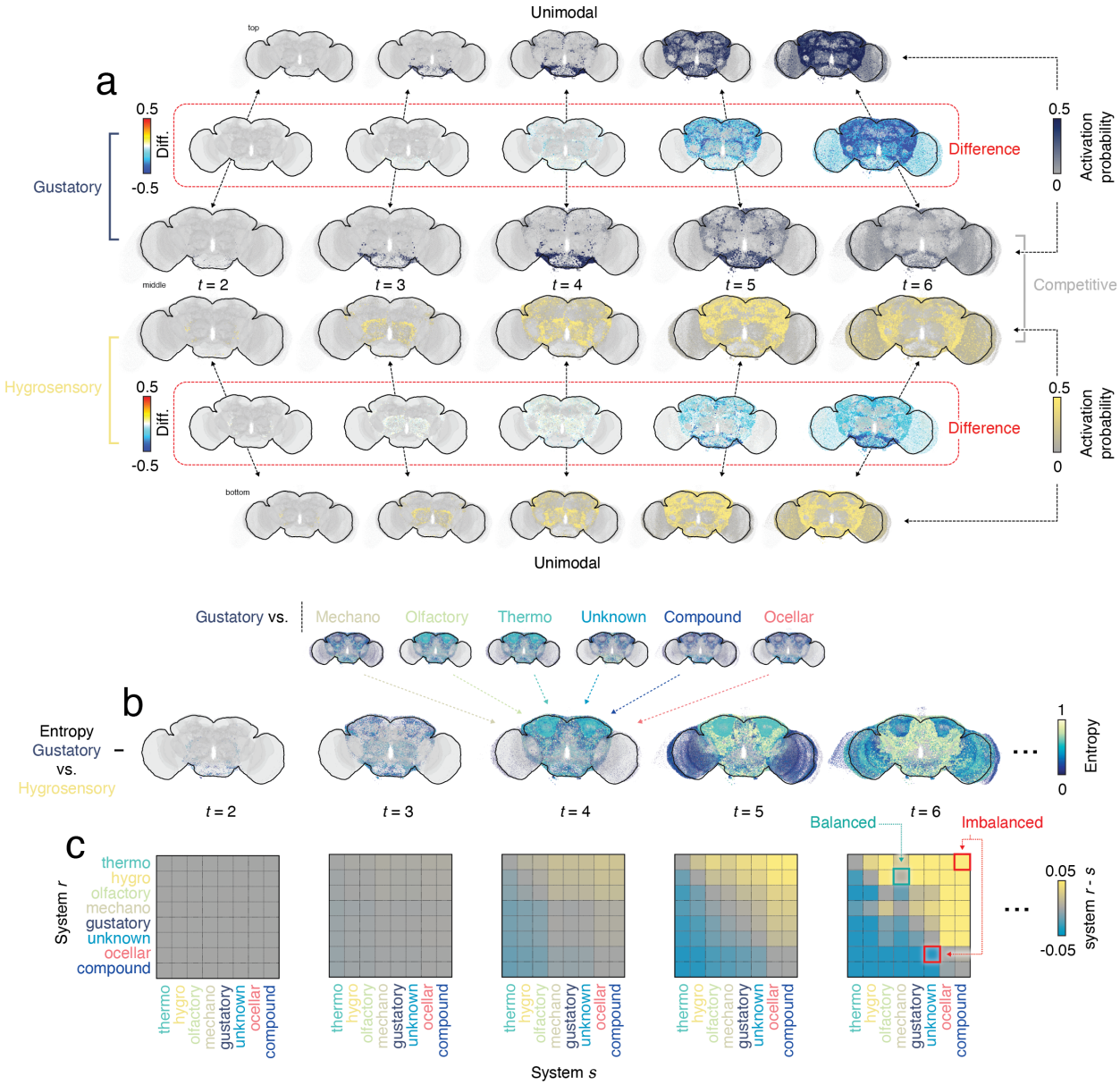

Figure 6. **Competitive cascade statistics.** (a) Comparison between unimodal gustatory and hygrosensory cascades (top and bottom) with competitive cascade (middle). (b) Entropy map for the gustatory and hygrosensory competitive cascade. High entropy neurons have "diverse" neighborhoods, i.e. their neighbors are activated by both gustatory and hygrosensory neurons. The inset with smaller brain maps depicts entropy maps of other competitive cascades involving the gustatory sensory modality at $t = 4$. (c) For every pair of neurons and at each time step, we calculated the relative dominance of one sensory modality over the other. That is, when we consider all active neurons, is one sensory modality over-expressed? Here, we plot this balance as a difference in proportion for all pairs of systems from time steps $t = 2$ to $t = 6$.

cascades, in which the set of seed neurons was assembled from neurons belonging to two different sensory systems. Following 1000 simulations, we calculated each neuron's mean activation time and compared this value to the activation time of the same neuron had we run the simulation for those same systems independently (see **Materials and Methods** for details). This allowed us to calculate the relative speed-up (reduction in activation time) due to cooperation.

In general, the mean reduction was always less than zero, although when averaged over all neurons, the magnitude was relatively small (mean reduction over all

system pairs of -0.11 ± 0.05 steps). The biggest reductions in activation time included the following pairs of sensory systems: gustatory+unknown (-0.18), olfactory+unknown (-0.18), compound+ocellar (-0.18), and gustatory+olfactory (-0.17) (Fig. 5a).

We also considered a more extreme cooperative scenario. Rather than simulate cascades in which pairs of sensory systems were seeded, we simulated pan-sensory cascades–i.e. *all* sensory systems are represented in the seed list. This scenario resulted in more extreme speed-ups (Fig. 5b); compared to unimodal cascades originating in compound visual or ocellar neurons, the pan-modality cascade reduced activation time by nearly 2 steps. For completeness, we show the reduction in activation time for each neuron in anatomical space (average over all eight sensory cascades; Fig. 5c). Again, we used enrichment analyses to link reductions in activation time with cellular annotations, demonstrating a broad correspondence neurobiology (Fig. 5d). Because the distribution of activation time reductions was heavy-tailed (a small number of neurons exhibited massive reductions while most exhibited more modest reductions), we focused on the top 1% of neurons, ordered by the reduction time. In Fig. 5e, we describe the makeup of these neurons, in terms of their annotations (raw counts rather than z-scores, as in the enrichment analysis).

Together, these results suggest visual sensory cascades, which exhibit dissimilar trajectories compared other sensory cascades, benefit the most from polysensory stimulation, exhibiting large reductions in activation time when co-seeded with other modalities. However, the average reduction in activation time for paired sensory cascades is modest, suggesting that, even independent uni-modal sensory cascades can take advantage of connectome architecture to rapidly spread from sensors to other neurons many steps across the brain.

Competitive sensory cascades

An alternative scenario for exploring interacting cascades is the so-called competitive cascade, wherein the signal propagated from two sensory modalities retains modal specificity. That is, neurons activated by either of these two modalities inherit the "label" of their respective sensory activator, maintaining the distinct identity of each signal. As with the cooperative cascade, the competitive cascade model can interpreted in terms of multisensory stimulation. However, unlike the cooperative case, where multiple sensory modalities amplified a signal, in the competitive scenario, the more "salient" of the two modalities can win out, effectively muting responses from the other modality. In this section, we report results under this competitive scenario.

As an illustrative example, we show distinctions between unimodal and competitive cascades originating in gustatory and hygrosensory neurons. In Fig. 6a (top+bottom), we show probabilistic activation maps corresponding to unimodal gustatory and hygrosensory cascades–i.e. without any competitive interaction. However, when we allow the cascades to evolve simultaneously and compete for territory, we find distinct spatiotemporal trajectories (Fig. 6a,middle). We highlight the distinctness by calculating the difference in activation probability (competitive minus unimodal).

One of the useful statistics that comes from the competitive cascades is the so-called "neighborhood entropy"–i.e. a summary statistic of how balanced a neuron's connected neighbors are in terms of their label. A neuron whose neighbors all have only a single label will have low entropy. In contrast, if the distribution of labels among neighbors is uniform, then the entropy will be large (see Fig. 6b for a depiction of entropy in anatomical space for the gustatory *versus* hygrosensory competitive cascade). Neurons with high values of entropy–bright colors–sit at the boundaries formed by two competing cascades. Thus, entropy serves as a useful and complementary measure for identifying locations where multiple (different) signals converge onto shared targets.

We estimated the "winning" sensory modality at each time step by calculating the imbalance in the number of neurons assigned to either label. In Fig. 6c, we show changes in this balance as a function of time step (note that the imbalance statistic has been normalized by the total number of neurons in the fly brain). Each entry in this plot corresponds to the difference in territory of sensory system r minus that of s. For example, at $t = 6$, we highlight two imbalanced competitive cascades (red). In the first case, thermosensary and compound visual systems are considered systems r and s, respectively. The bright yellow entry indicates that system r occupies more territory than system s at time $t = 6$. The second case considers ocellar and unknown sensory systems as r and s, respectively. The blue entry indicates that system r occupies less territory than s. We also show a balanced case (hygrosensory *versus* mechanosensory) where the two cascades are in relative balance at $t = 6$.

This competitive cascade model helps us to better understand multisensory integration in a directed and weighted connectome. For instance, aside from imbalances, we can use the neighborhood entropy measure to track the formation of "boundaries" or "fronts" between the competing cascades. High entropy neurons, by definition, are surrounded by multiple labels and therefore positioned within the network for multisensory integration. Moreover, because the *Drosophila* connectome is directed, we can define neighborhoods based on pre-/post-synaptic connectivity (or both). High levels of pre-/post-synaptic entropy correspond to neurons re-

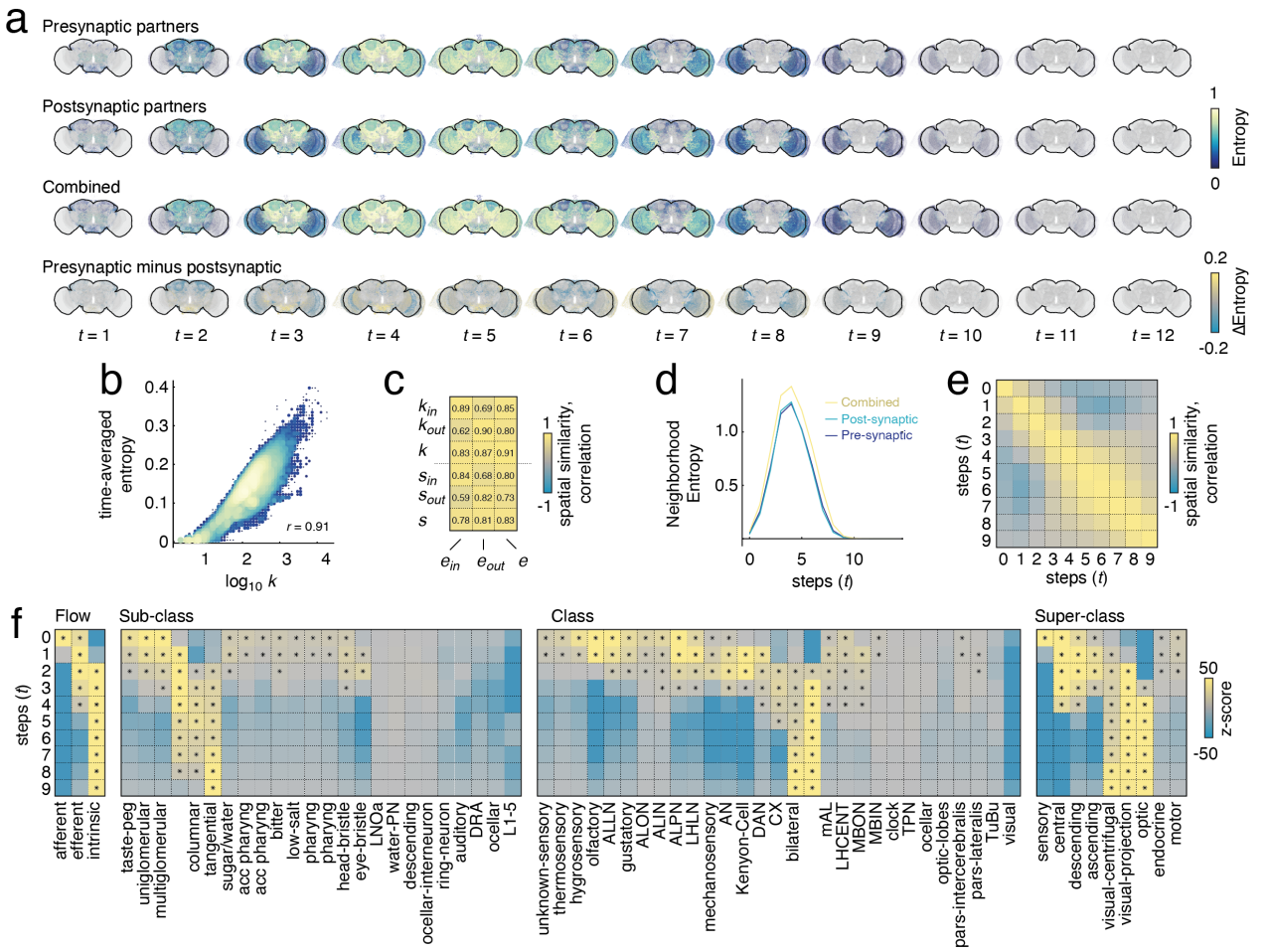

Figure 7. **Additional competitive cascade statistics.** The entropy patterns vary depending upon how one defines a neuron's "neighborhood". For instance, one can define a neighborhood based on a neuron's pre- or post-synaptic neighbors or the combined neighborhood. Here, we compare these three definitions in panel *a*. We also related entropy to conventional network statistics. (*b*) Scatterplot of time-averaged entropy against the logarithm of nodes' total degrees. (*c*) Correlation of entropy with various other network statistics: in/out/total degree and strength. (*d*) Mean whole-brain entropy of different neighborhood definitions as a function of step. (*e*) Similarity of whole-brain combined-neighborhood entropy patterns between time steps $t = 0$ to $t = 9$. (*f*) Enrichment statistics for whole-brain combined-neighborhood entropy.

ceiving input from a diverse pool of neurons (based on their activation label) or delivering their output into a heterogeneous/diverse population. Here, we estimated these measures using a pan-sensory competitive cascade model, wherein *all* sensory modalities were included among the seed list (and represented equally; Fig. 7a). Although we found the three entropy measures to be highly correlated (mean pairwise similarity across all time points $r = 0.81 \pm 0.21$), we nonetheless identified subtle, although distinct, differences between entropies computed based on pre- and post-synaptic partners (Fig. 7a). The subtlety of these differences likely reflects the strong correlation between nodes incoming and outgoing degree ($r = 0.82$). Indeed, when we averaged the combined-degree neuronal entropy across time, we found that it was strongly correlated with neurons' total degrees ($r = 0.91$; Fig. 7b). Entropy scores were, in general, strongly correlated with both binary and weighted degree (Fig. 7c), positing "hubness" as a structural analog of neighborhood entropy. Nonetheless, collapsing entropy patterns across time obscures the temporal variation in the measure. Globally, the mean entropy follows a variable trajectory, increasing rapidly to a peak at step 5 before decreasing to zero (Fig. 7d). Moreover, the spatial similarity of those patterns are variable; although temporally adjacent entropy maps

are correlated, over roughly the first five steps, the maps are uncorrelated, and entropy maps at later steps are even anti-correlated with those from the first several steps (Fig. 7e), suggesting a more complex and time-dependent relationship with the underlying network.

Finally, we examined the enrichment patterns of neighborhood entropy within different annotation labels. As with activation time and convergence zone reported in the previous subsections, we found evidence that entropy enrichment followed distinct temporal trajectories based on annotation. Afferent sensory neurons all exhibit high levels of entropy within the first two steps. These initial peaks were followed enrichment of efferent and intrinsic neurons, including columnar neurons, Kenyon cells, neurons in the central complex, ascending/descending neurons, and eventually visual centrifugal/projection neurons (Fig. 7f).

These observations, in line with measures of convergence presented in earlier sections, point towards intrinsic neurons in the central brain as potential sensory integration sites. These neurons are situated at the boundaries of competing "flows" and exhibit high levels of entropy. Importantly, we find that a neuron's role as integrator (as indexed by its neighborhood entropy) is, on average, correlated with its degree, but in general varies over time, underscoring the fact that a neuron's functional role may depend upon explicitly upon context (in this case timing with respect to stimulus onset).

Data-driven clustering of neurons based on cascade properties

Previously, we described a series of summary statistics derived from the spatiotemporal evolution of cascades. These measures include estimates of activation time, convergence, competitiveness, and activation time reduction. We then used an enrichment analysis to link those measures with neurobiological annotations. Here, rather than align with known measures, we seek to partition neurons into clusters based explicitly on metrics derived from cascades.

Briefly, we aggregated measures of convergence, entropy (from the competitive cascades), reduction time (from cooperative cascades), and activation timing into a $N \times N_{features}$ matrix. We then standardized (z-scored) each column and used k-means clustering with a correlation metric to partition neurons into groups (Fig. 8a). We varied the number of clusters from 1-50 and measured squared sum of errors at each k (100 random restarts). We found that $k = 6$ clusters represented an optimal number of clusters (an "elbow" in terms of error; see Fig. 8b for representations of the clusters in anatomical space).

The clustering algorithm returned a distinct centroid – typical profile of cascade metrics – for each of the six clusters (Fig. 8c). For example, cluster 1 (yellow) exhibited the earliest activation time on average, which it paired with early levels of relatively high entropy. We then ask which annotations were enriched for the cluster 1 label. As expected, cluster 1 was composed of, mostly, afferent, sensory, and ascending neurons, agreeing with the cluster centroids positioning this cluster as the progenitor of cascades. Cluster 2 (pink) followed in time, peaking in convergence zone, entropy, and activation time between steps $t = 3$ and $t = 6$. It was composed most of efferent, multi-/uni-glomerular neurons, as well as a number of central complex interneruons–e.g. Kenyon cells. The remaining clusters evolved sequentially in terms of their mean activation time. As with clusters 1 and 2, clusters 3-6 exhibited distinct enrichment patterns, all enriched within intrinsic neurons and converging on visual projection/centrifugal neurons in the optic lobes.

These observations suggest that spreading dynamics constrained by the connectome can be used to categorize neurons. The categories reported here can be temporally ordered, so that the grouping correspond to neurons with similar timing in terms of their activations and their convergence, competition, and cooperation with one another.

Additional analyses

We also performed several supplementary analyses not included in the main text. First, we showed that our results changed little if we were to threshold weak synapses (retaining only connections corresponding to 5 or more synapses). We found that mean activation times, cooperative speed-ups, and neighborhood entropy scores were highly correlated (Spearman correlations of $\rho_{act} = 0.80$; $\rho_{coop} = 0.56$; $\rho_{comp} = 0.82$; all estimated with $p_{transmission} = 0.01$ and $N_{seed} = 16$). Second, we show that activation timing is not directly predicted based on path length alone (a measure derived directly from connectivity [55]; Fig. S3). Third, we tracked activations by neurotransmitter type, identifying neurotransmitter-specific activation times (Fig. S4). Fourth, we demonstrated that activation times during sensory cascades are distinct from cascades seeded in other, non-sensory neurons (Fig. S5). Fifth, we decomposed the connectome into communities using a nested stochastic blockmodel [56, 57] (see Mehta et al. [58], [59], and González-Montesino et al. [60] for other views). We showed that statistics derived from the cascades respect community boundaries and are highly enriched within communities (Fig. S6 and Fig. S7). As a continuous alternative to the hard partitions derived during community detection, we also performed a principal components analysis, identifying brain-wide gradi-

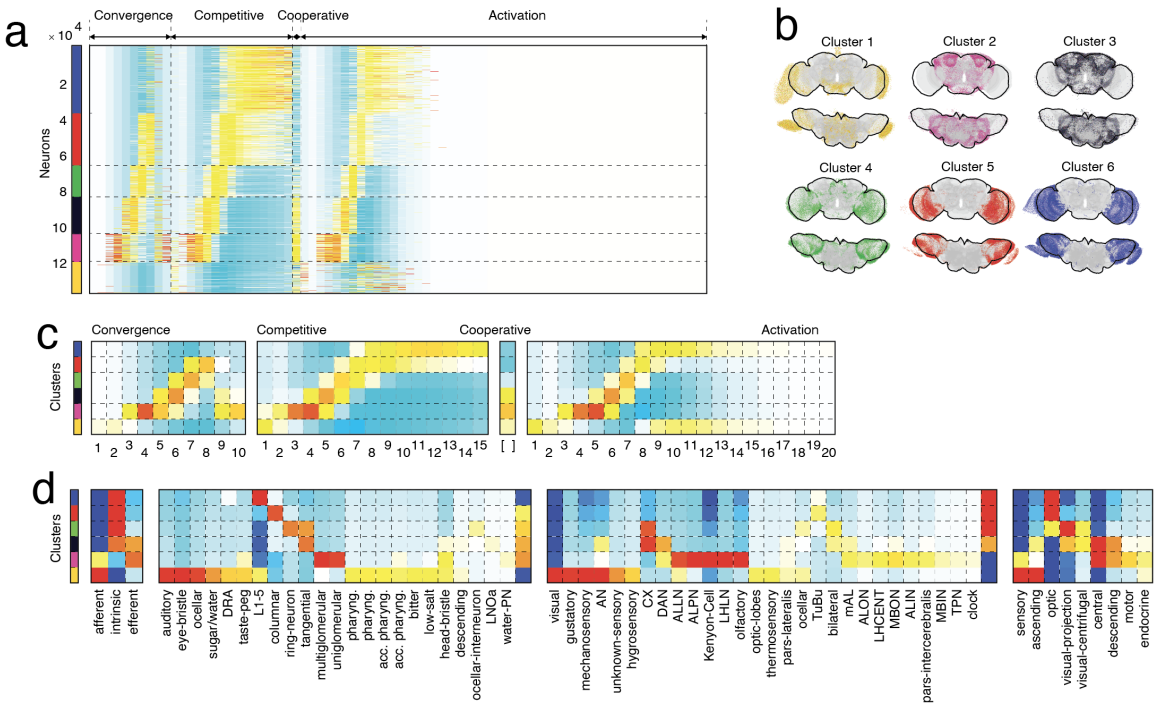

Figure 8. **Clustering neurons based on their cascade properties.** (*a*) Neurons ordered by cluster assignment. Columns correspond to z-scored cascade metrics. (*b*) Cluster labels depicted in anatomical space. (*c*) Cluster centroids. (*d*) Enrichment of cluster labels across annotations.

ents corresponding to modes of variation across cascade statistics (Fig. S8).

DISCUSSION

The *Drosophila* connectome contains approximately 140,000 neurons and 15 million binary connections. These connections constrain communication and signaling patterns between neurons, ultimately supporting brain function. Occasionally, we can glean insight into those functions directly from the connectome alone. For instance, we showed that sensory neurons are highly segregated from one another–i.e. very few direct synapses exist between different sensory modalities. This architectural feature, we speculate, helps support specialized and parallel processing of sensory signals.

However many functions require integrating information from different areas in order to make decisions [61], successfully navigate an environment [62], and to plan and execute actions [63]. These types of integrative behaviors are likely supported by multi-step (synaptic links) circuits and not immediately identifiable from the direct connections encoded in the connectome. Instead, these circuits must be inferred experimentally through direct perturbations [9] or through *in silico* simulations of connectome-constrained dynamics [27, 28, 64, 65].

Indeed, this intuition–gleaning insight into function by studying multi-step pathways–is one of the aims of this paper, and one that we elect to address dynamically. Although there exist many different "flavors" of dynamic models–e.g. biophysically realistic dynamical models (with varying degrees of complexity) [66, 67]–here we study a spreading model grounded in network science. This model abstracts away biophysical realism, replacing it with tractability and interpretability, thus allowing us to unambiguously track the evolution of signaling cascades through the fly brain.

Variants of the spreading model have been studied elsewhere, providing insight into signal spread in the human connectome [31] and in both the larval *Drosophila* [52] and adult *Drosophila* connectomes [36, 68] (although never at the scale of the entire connectome).

Our findings using this model suggest that although sensory information is initially processed in parallel, it quickly converges onto a common set of secondary targets, irrespective of the sensory modality in which it originates. These secondary targets are situated in the central complex, but also include motor and descending

neurons, suggesting further that effectors are positioned only a few synaptic links from sensors.

Our work also makes testable predictions about polysensory integration. For instance, using the convergence index, we show that hygrosensation and thermosensation consistently activate overlapping sets neurons. The hypothesis that these groups of neurons are integration sites could be tested experimentally through paired sensory stimulation [63, 69–71]. The same is true of the triplets, quartets, and so on, although scaling multisensory paradigms beyond paired stimuli may present experimental challenges.

Another key component of the spreading model is that its evolution is entirely passive–i.e. in its current form, the spreading of activation requires no explicit direction, guidance, or control signals [72–76]. The spatiotemporal trajectories of sensory cascades are a consequence of the connectome's wiring (and the dynamics), suggesting that the connectome may be, in part, configured to support sensory-to-effector pathways.

Future work should continue to investigate dynamic implications of the connectome. This work should include both experimental components–e.g. registering spontaneous and stimulus-evoked recordings with projectome-level connectivity [77] to better understand the interplay between structure and function [8, 78, 79]–as well as simulation to generate experimentally testable hypotheses the functional coupling between neurons or activation patterns [64, 80]. Note that this line of work–i.e. prediction of function from structure–is an already extremely fruitful sub-discipline in macro-/meso-scale network neuroscience [77].

There are multiple opportunities for improving the realism of the spreading model. For example, here we deliberately ignored the valence of synapses (excitatory *versus* inhibitory) as well as the neurotransmitter type [81]. Incorporating these and other neurobiological features into the model would enhance its realism while preserving the interpretability of the spreading model. Further, we used synapse count as a proxy for weight. However, recent studies that sought to learn synaptic weights, found that the learned weights generally disagreed with the synapse count [28]. Finally, missing from our study is the ventral nerve cord and motor neurons [82]. Incorporating these additional elements could help us to understand how sensory signals are transformed into motor outputs [83, 84].

Finally, our study has important implications for connectomics and network neuroscience. Although network science tools can be applied to brain network data at any spatiotemporal scale (in principle), it has been most effectively applied to meso- and macro-scale network data. At that resolution, networks are often constructed for entire brains (as well as peripheral structures [85]), quickly, with relatively little expense, and for both humans as well as non-human mammals [86–88]. Accordingly, the hallmark features of those networks (and insight into their functions) has been documented [89] and include short processing paths [90, 91], heterogeneous degree distributions [5], rich-clubs [24, 92], modular structure [93–95], and cost-efficient embedding [96, 97]. However, how synaptic connectivity at finer scales contributes to these larger-scale features is not clear (at least not at the whole-brain level). Our work complements other contemporary applications of network science to synapse-level connectomes seeking connectivity features analogous to those at the meso-/macro-scale, but also presenting opportunities to discover entirely new types of organization [98–100].

MATERIALS AND METHODS

Drosophila connectome dataset

All connectome data, including synaptic connectivity, three-dimensional coordinates, neuropil volumes, and annotations were obtained from `https://codex.flywire.ai/`. These derivatives represent the output of a process beginning with nanometer-resolution electron microscopy images of an adult female *Drosophila* [101]. The FlyWire project allowed citizen scientists to trace neurons [39] to reconstruct the connectome. Combined with automated approaches [102, 103], the end result was a complete map of synaptic connections among approximately 139,000 neurons.

Neurons in *Drosophila* are polyadic, thus the same pair of neurons can synapse onto one another at multiple distinct sites. The `https://codex.flywire.ai/` are shared in two versions: one in which pairs of neurons were connected if they were linked by, at minimum, five synapses and another in which even a single synapse was considered evidence that two neurons were connected (unthresholded). In the main text, we analyze the unthresholded connectome, but note that results are consistent with those obtained using the thresholded version.

Annotation data were obtained from at the same time as the connectome data. Annotations were grouped into four distinct categories [48]. The first two annotations are "dense," in the sense that every neuron is assigned a label.

1. "Flow": afferent, efferent, intrinsic.

2. "Super-class": sensory (periphery to brain), motor (brain to periphery), endocrine (brain to corpora allata/cardiaca), ascending (ventral nerve cord (VNC) to brain), descending (brain to VNC), visual projection (optic lobes to central brain), visual centrifugal (central brain to optic lobes), or intrinsic to the optic lobes or the central brain

The other two categories are not dense–i.e. not all neurons are assigned a label. The "Class" and "Subclass" annotations are nested hierarchically within the the parent "Super-class" and describe cell groups reported in the extant literature, e.g. neurons in the optic lobe [104].

Cascade model

Here we explore an abstract cascade model. In this model, each neuron exists in one of three states: active, inactive, or quiescent. In our simulations, we set select sets of neurons to be active at time $t = 0$. These initially activated neurons are referred to as "seeds" and are selected from among sensory neurons alone. The seeds are intended to represent sensory stimuli.

In this model, neurons that are active at time t probabilistically activate their post-synaptic partners at $t+1$. Suppose neuron i makes a single synapse onto neuron j. Given that i is active at t, the probability that neuron i activates j at $t+1$ is given by the transmission probability parameter, $p_{transmission}$. Conversely, the probability that i does *not* activate j is simply $q = 1 - p_{transmission}$.

Oftentimes, neuron i makes multiple synapses onto j. We treat these as independent trials; only one successful trial is sufficient to activate neuron j. What is the probability that at least one event is successful? In the space of possible outcomes, there is exactly one outcome in which none of the synapses successfully activate j. Its probability is given by: $q^{\#synapses} = (1 - p_{transmission})^{\#synapses}$. All other possibly outcomes include at least one successful transmission event. Hence, the probability that j is activated by neuron i at time $t+1$ is given by: $1 - q^{\#synapses}$.

Activation probability

The cascade model is stochastic. In principle, each run can yield a different sequence of neuronal activations. For every experiment, we summarize across 1000 independent runs by estimating the probability a given neuron was active at time t (see Fig. S1 for example maps). We denote the activation probability of neuron i at time t as $P_i(t)$. In the main text we describe several statistics calculated directly from the probabilistic activation curves.

Dominance maps

We use the cascade model to simulate sensory cascades by allowing a fixed number of sensory neurons with specific modalities to be active at time $t = 0$. In total, we consider eight sensory modalities as determined by hierarchical annotations of sensory neurons: thermosensation, hygrosensation, olfaction, mechanosensation, gustation, vision (ocellar and compound), and an unknown sensory class (no clear assignment). For estimate modality-specific activation probability curves for each neuron. Given that sensory neurons associated with modality m were seeded at time $t = 0$, we denote the probability that neuron i is active at time t as: $P_i^m(t)$. From these estimates, can calculate the "dominant" modality for each neuron at any given timepoint as the m that maximizes $P_i^m(t)$.

Convergence index

The dominance index represents a "winner take all" measure, ascribing dominance to a single sensory modality. In reality, there could be multiple near-maximal modalities, all with similar activation probabilities. To account for this possibility, we defined the convergence index. Specifically, we define a threshold, τ, and calculate: $C_i(t) = \sum_m [P_i^m(t) \geq \tau]$. That is, we count the number of sensory modalities for which the activation probability of node i at time t is at least τ.

Cooperative cascades

We explored several variations of the cascade model. The first variant focused on "unimodal" cascades, wherein the seed neurons were selected from among a single sensory modality. However, we also considered a second "cooperative" variant, in which pairs of sensory systems were seeded (doubling the total number of seed neurons). We then calculated the reduction in the mean activation time (speed-up) as a result of the dual-seed approach as: $A_{rs} - \min(A_r, A_s)$, where A_{rs} is the activation time of a given neuron under the cooperative, dual-seed model A_r and A_s are the activation times of the same neuron under the unimodal model where modalities r and s were seeded independently.

Competitive cascades

We also considered a "competitive" variant of the cascade model. In this case, we imagine two distinct sensory signals ("blue" and "red") spreading throughout the connectome carrying distinct information. Post-synaptic neurons activated by a majority blue/red pre-synaptic neurons will be blue/red at the following timestep. In the rare event of a tie–i.e. equal number of red and blue activating neurons–the post-synaptic neu-

ron becomes blue/red at the following timestep with equal probability.

Neighborhood entropy

Under the competitive model, we can calculate an entropy measure that describes whether a node is positioned in the network so that its neighbors are mostly homogeneous in terms of their redness/blueness or whether their neighbors are diverse. To do this, we identify each neuron's connected neighbors and, for at time t, those the proportion of those that are active and are blue/red. We then rescale these values so that their total sums to 1, and calculate an entropy, $H_i(t) = -p_{blue}log_2(p_{blue}) + -p_{red}log_2(p_{red})$. Intuitively, when this entropy is close to 1, it implies that the distribution of blue/red neighbors is approximately equal. However, values close to zero imply that one of the two colors is more dominant.

An important consideration is how one defines "neighborhood" in this context. In the main text, we consider three possibilities: a neuron's pre-synaptic partners, its post-synaptic partners, and the union of those two sets.

Note that in all of the above calculations, we disregard inactive or quiescent neurons. That is, only active neurons contribute to the entropy scores.

Community detection

Many studies have shown that biological neural networks at varying spatial scales can be meaningfully partitioned into clusters or communities [5, 57, 94, 95, 105–110]. In general, community structure is unknown ahead of time and must be estimated or inferred algorithmically. The procedure is referred to as community detection [111], and there exist many approaches for doing so [112–117], each of which makes specific assumptions about what constitutes a community.

One of the oldest approaches for community detection is the stochastic blockmodel [118–122]. Briefly, blockmodels imagine that every node in the network is assigned a label. The probability that any pair of nodes are connected and the weight of that connection depends only upon the communities to which they are assigned. In general, blockmodels estimate community labels and connection probability/weight distributions so as to maximize the likelihood that the model generated the observed network.

Recently, there has been renewed interest in the application of blockmodels to brain network data [22, 109, 123–130]. Here, we leverage a nested and weighted variant of the classical blockmodel to partition the *Drosophila* connectome into hierarchical communities [56]. Using this model, we obtained an estimate of the consensus hierarchical partition using a Markov Chain Monte Carlo procedure [131]. Briefly, this procedure entails allowing the Markov chain to equilibriate and sampling 10000 high-quality partitions. These partitions are aligned to one another to discover latent "modes" – partitions that share many characteristics with one another [132]. From these modes, we obtained for each neuron the community it was most likely assigned to. All analyses using communities were carried out on the resulting partition (Fig. S6 and Fig. S7).

Clustering based on cascade properties

In the main text, we derived a series of statistics for neurons based on their activation times, convergence, neighborhood entropies, and speed-ups. We can use these data to partition neurons into clusters based not on their connectivity (information derived from the connectome) but these dynamic, cascade-based properties.

To do this, we constructed a $[N \times F]$ matrix, where N is the number of nodes and $F = 27$ is the total number of features. In this case, we considered the following features derived from omnibus sensory cascades–i.e. where all sensory modalities were seeded:

1. **Activation probability**: The $[N \times 1]$ vector of each neuron's mean activation time.
2. **Convergence index**: The $[N \times 10]$ array of neurons' convergence indices over the first 10 time steps.
3. **Neighborhood entropy**: The $[N \times 15]$ array of neurons' neighborhood entropy (estimated using both pre-/post-synaptic partners).
4. **Speed up**: The $[N \times 1]$ vector of speed-ups (reductions in activation times) from single-modality unimodal cascades to the omnibus cascade.

To cluster these data, every column was standardized (z-scored). We then used k-means clustering to assign neurons to a unique cluster [133]. We selected the optimal number of clusters based on the inflection point in the summed square errors of cluster centroids relative to their constituents. Based on these analyses, we identified $k = 6$ as the optimal number of clusters.

Annotation enrichment analysis

Throughout this manuscript we describe an "enrichment" procedure for linking continuous data to categorical labels–e.g. annotations. The aim of this procedure, in more detail, was to determine if a particular variable

was over-expressed (enriched) within a given annotation category. To do this, we calculated the variable of interest's mean value within all neurons associated with a specific annotation. We then randomly permuted the annotation labels (keeping the total number constant) and calculated the new mean. We repeated this procedure 1000 times, generated a null distribution of mean values. The enrichment score for that variable within that annotation category is the original mean expressed as a z-score with respect to the null distribution.

ACKNOWLEDGEMENTS

Data and code availability statement

All data are publicly available through `https://codex.flywire.ai/` with no restrictions. Code is available upon request.

[1] Olaf Sporns, Giulio Tononi, and Rolf Kötter. The human connectome: a structural description of the human brain. *PLoS Comput Biol*, 1(4):e42, 2005.

[2] Seung Wook Oh, Julie A Harris, Lydia Ng, Brent Winslow, Nicholas Cain, Stefan Mihalas, Quanxin Wang, Chris Lau, Leonard Kuan, Alex M Henry, et al. A mesoscale connectome of the mouse brain. *Nature*, 508(7495):207–214, 2014.

[3] Larry W Swanson, Joel D Hahn, and Olaf Sporns. Organizing principles for the cerebral cortex network of commissural and association connections. *Proceedings of the National Academy of Sciences*, 114(45):E9692–E9701, 2017.

[4] Nikola T Markov, MM Ercsey-Ravasz, AR Ribeiro Gomes, Camille Lamy, Loic Magrou, Julien Vezoli, P Misery, A Falchier, R Quilodran, MA Gariel, et al. A weighted and directed interareal connectivity matrix for macaque cerebral cortex. *Cerebral cortex*, 24(1):17–36, 2014.

[5] Patric Hagmann, Leila Cammoun, Xavier Gigandet, Reto Meuli, Christopher J Honey, Van J Wedeen, and Olaf Sporns. Mapping the structural core of human cerebral cortex. *PLoS Biol*, 6(7):e159, 2008.

[6] Sven Maximilian Dorkenwald. *Analysis of Neuronal Wiring Diagrams*. Princeton University, 2023.

[7] Andrea Avena-Koenigsberger, Bratislav Misic, and Olaf Sporns. Communication dynamics in complex brain networks. *Nature Reviews Neuroscience*, 19(1): 17, 2018.

[8] Maxwell H Turner, Kevin Mann, and Thomas R Clandinin. The connectome predicts resting-state functional connectivity across the drosophila brain. *Current Biology*, 2021.

[9] Francesco Randi, Anuj K Sharma, Sophie Dvali, and Andrew M Leifer. Neural signal propagation atlas of caenorhabditis elegans. *Nature*, 623(7986):406–414, 2023.

[10] Caio Seguin, Olaf Sporns, and Andrew Zalesky. Brain network communication: concepts, models and applications. *Nature Reviews Neuroscience*, pages 1–18, 2023.

[11] Cornelia I Bargmann and Eve Marder. From the connectome to brain function. *Nature methods*, 10(6):483–490, 2013.

[12] Hae-Jeong Park and Karl Friston. Structural and functional brain networks: from connections to cognition. *Science*, 342(6158), 2013.

[13] Stéphane Molotchnikoff, Vishal Bharmauria, Lyes Bachatene, Nayan Chanauria, and Jose Fernando Maya-Vetencourt. The function of connectomes in encoding sensory stimuli. *Progress in Neurobiology*, 181: 101659, 2019.

[14] Nadine Randel, Albina Asadulina, Luis A Bezares-Calderón, Csaba Verasztó, Elizabeth A Williams, Markus Conzelmann, Réza Shahidi, and Gáspár Jékely. Neuronal connectome of a sensory-motor circuit for visual navigation. *elife*, 3:e02730, 2014.

[15] Danielle S Bassett and Olaf Sporns. Network neuroscience. *Nature neuroscience*, 20(3):353–364, 2017.

[16] Joshua K Wong, Erik H Middlebrooks, Sanjeet S Grewal, Leonardo Almeida, Christopher W Hess, and Michael S Okun. A comprehensive review of brain connectomics and imaging to improve deep brain stimulation outcomes. *Movement Disorders*, 35(5):741–751, 2020.

[17] Ed Bullmore and Olaf Sporns. Complex brain networks: graph theoretical analysis of structural and functional systems. *Nature reviews neuroscience*, 10 (3):186–198, 2009.

[18] Albert Lin, Runzhe Yang, Sven Dorkenwald, Arie Matsliah, Amy R Sterling, Philipp Schlegel, Szi-chieh Yu, Claire E McKellar, Marta Costa, Katharina Eichler, et al. Network statistics of the whole-brain connectome of drosophila. *Nature*, 634(8032):153–165, 2024.

[19] Mikail Rubinov and Olaf Sporns. Complex network measures of brain connectivity: uses and interpretations. *Neuroimage*, 52(3):1059–1069, 2010.

[20] Chi-Tin Shih, Olaf Sporns, Shou-Li Yuan, Ta-Shun Su, Yen-Jen Lin, Chao-Chun Chuang, Ting-Yuan Wang, Chung-Chuang Lo, Ralph J Greenspan, and Ann-Shyn Chiang. Connectomics-based analysis of information flow in the drosophila brain. *Current Biology*, 25(10): 1249–1258, 2015.

[21] Balazs Pentek and Maria Ercsey-Ravasz. The exponential distance rule based network model predicts topology and reveals functionally relevant properties of the drosophila projectome. *arXiv preprint arXiv:2410.01269*, 2024.

[22] Richard F Betzel, John D Medaglia, and Danielle S Bassett. Diversity of meso-scale architecture in human and non-human connectomes. *Nature communications*, 9(1):1–14, 2018.

[23] Richard F Betzel and Danielle S Bassett. Specificity and robustness of long-distance connections in weighted, interareal connectomes. *Proceedings of the National Academy of Sciences*, 115(21):E4880–E4889, 2018.

[24] Logan Harriger, Martijn P Van Den Heuvel, and Olaf Sporns. Rich club organization of macaque cerebral cortex and its role in network communication. 2012.

[25] Martijn P Van den Heuvel, Edward T Bullmore, and Olaf Sporns. Comparative connectomics. *Trends in cognitive sciences*, 20(5):345–361, 2016.

[26] Gustavo Deco, Viktor K Jirsa, Peter A Robinson, Michael Breakspear, and Karl Friston. The dynamic brain: from spiking neurons to neural masses and cortical fields. *PLoS computational biology*, 4(8): e1000092, 2008.

[27] Michael Breakspear. Dynamic models of large-scale brain activity. *Nature neuroscience*, 20(3):340–352, 2017.

[28] Janne K Lappalainen, Fabian D Tschopp, Sridhama Prakhya, Mason McGill, Aljoscha Nern, Kazunori Shinomiya, Shin-ya Takemura, Eyal Gruntman, Jakob H Macke, and Srinivas C Turaga. Connectome-constrained networks predict neural activity across the fly visual system. *Nature*, pages 1–9, 2024.

[29] James C Pang, Kevin M Aquino, Marianne Oldehinkel, Peter A Robinson, Ben D Fulcher, Michael Breakspear, and Alex Fornito. Geometric constraints on human brain function. *Nature*, 618(7965):566–574, 2023.

[30] Joaquín Goñi, Martijn P Van Den Heuvel, Andrea Avena-Koenigsberger, Nieves Velez De Mendizabal, Richard F Betzel, Alessandra Griffa, Patric Hagmann, Bernat Corominas-Murtra, Jean-Philippe Thiran, and Olaf Sporns. Resting-brain functional connectivity predicted by analytic measures of network communication. *Proceedings of the National Academy of Sciences*, 111(2):833–838, 2014.

[31] Bratislav Mišić, Richard F Betzel, Azadeh Nematzadeh, Joaquin Goni, Alessandra Griffa, Patric Hagmann, Alessandro Flammini, Yong-Yeol Ahn, and Olaf Sporns. Cooperative and competitive spreading dynamics on the human connectome. *Neuron*, 86(6): 1518–1529, 2015.

[32] Duncan J Watts. A simple model of global cascades on random networks. *Proceedings of the National Academy of Sciences*, 99(9):5766–5771, 2002.

[33] Mark Granovetter. Threshold models of collective behavior. *American journal of sociology*, 83(6):1420–1443, 1978.

[34] Reuben O'Dea, Jonathan J Crofts, and Marcus Kaiser. Spreading dynamics on spatially constrained complex brain networks. *Journal of the Royal Society Interface*, 10(81):20130016, 2013.

[35] Kamal Shadi, Eva Dyer, and Constantine Dovrolis. Multisensory integration in the mouse cortical connectome using a network diffusion model. *Network Neuroscience*, 4(4):1030–1054, 2020.

[36] Jacob C Worrell, Jeffrey Rumschlag, Richard F Betzel, Olaf Sporns, and Bratislav Mišić. Optimized connectome architecture for sensory-motor integration. *Network Neuroscience*, 1(4):415–430, 2017.

[37] John G White, Eileen Southgate, J Nichol Thomson, and Sydney Brenner. The structure of the nervous system of the nematode caenorhabditis elegans. *Philos Trans R Soc Lond B Biol Sci*, 314(1165):1–340, 1986.

[38] Moritz Helmstaedter, Kevin L Briggman, Srinivas C Turaga, Viren Jain, H Sebastian Seung, and Winfried Denk. Connectomic reconstruction of the inner plexiform layer in the mouse retina. *Nature*, 500(7461): 168–174, 2013.

[39] Sven Dorkenwald, Claire E McKellar, Thomas Macrina, Nico Kemnitz, Kisuk Lee, Ran Lu, Jingpeng Wu, Sergiy Popovych, Eric Mitchell, Barak Nehoran, et al. Flywire: online community for whole-brain connectomics. *Nature methods*, 19(1):119–128, 2022.

[40] Ann-Shyn Chiang, Chih-Yung Lin, Chao-Chun Chuang, Hsiu-Ming Chang, Chang-Huain Hsieh, Chang-Wei Yeh, Chi-Tin Shih, Jian-Jheng Wu, Guo-Tzau Wang, Yung-Chang Chen, et al. Three-dimensional reconstruction of brain-wide wiring networks in drosophila at single-cell resolution. *Current biology*, 21(1):1–11, 2011.

[41] Alexander Shapson-Coe, Michał Januszewski, Daniel R Berger, Art Pope, Yuelong Wu, Tim Blakely, Richard L Schalek, Peter H Li, Shuohong Wang, Jeremy Maitin-Shepard, et al. A petavoxel fragment of human cerebral cortex reconstructed at nanoscale resolution. *Science*, 384(6696):eadk4858, 2024.

[42] Lidia Ripoll-Sánchez, Jan Watteyne, HaoSheng Sun, Robert Fernandez, Seth R Taylor, Alexis Weinreb, Barry L Bentley, Marc Hammarlund, David M Miller, Oliver Hobert, et al. The neuropeptidergic connectome of c. elegans. *Neuron*, 111(22):3570–3589, 2023.

[43] Aljoscha Nern, Frank Loesche, Shin-ya Takemura, Laura E Burnett, Marisa Dreher, Eyal Gruntman, Judith Hoeller, Gary B Huang, Michał Januszewski, Nathan C Klapoetke, et al. Connectome-driven neural inventory of a complete visual system. *bioRxiv*, 2024.

[44] Larry F Abbott, Davi D Bock, Edward M Callaway, Winfried Denk, Catherine Dulac, Adrienne L Fairhall, Ila Fiete, Kristen M Harris, Moritz Helmstaedter, Viren Jain, et al. The mind of a mouse. *Cell*, 182 (6):1372–1376, 2020.

[45] Csaba Verasztó, Sanja Jasek, Martin Gühmann, Réza Shahidi, Nobuo Ueda, James David Beard, Sara Mendes, Konrad Heinz, Luis Alberto Bezares-Calderón, Elizabeth Williams, et al. Whole-animal connectome and cell-type complement of the three-segmented platynereis dumerilii larva. *BioRxiv*, pages 2020–08, 2020.

[46] Mojtaba R Tavakoli, Julia Lyudchik, Michał Januszewski, Vitali Vistunou, Nathalie Agudelo, Jakob Vorlaufer, Christoph Sommer, Caroline Kreuzinger, Barbara Oliveira, Alban Cenameri, et al. Light-microscopy based dense connectomic reconstruction of mammalian brain tissue. *bioRxiv*, pages 2024–03, 2024.

[47] Sven Dorkenwald, Arie Matsliah, Amy R Sterling, Philipp Schlegel, Szi-Chieh Yu, Claire E McKellar, Al-

bert Lin, Marta Costa, Katharina Eichler, Yijie Yin, et al. Neuronal wiring diagram of an adult brain. *Nature*, 634(8032):124–138, 2024.

[48] Philipp Schlegel, Yijie Yin, Alexander S Bates, Sven Dorkenwald, Katharina Eichler, Paul Brooks, Daniel S Han, Marina Gkantia, Marcia Dos Santos, Eva J Munnelly, et al. Whole-brain annotation and multi-connectome cell typing of drosophila. *Nature*, 634 (8032):139–152, 2024.

[49] Nicole K Guittari, Miguel E Wimbish, Patricia K Rivlin, Mark A Hinton, Jordan K Matelsky, Victoria A Rose, Jorge L Rivera Jr, Nicole E Stock, Brock A Wester, Erik C Johnson, et al. Nanoscale connectomics annotation standards framework. *arXiv preprint arXiv:2410.22320*, 2024.

[50] Alessandro Motta, Meike Schurr, Benedikt Staffler, and Moritz Helmstaedter. Big data in nanoscale connectomics, and the greed for training labels. *Current opinion in neurobiology*, 55:180–187, 2019.

[51] Louis K Scheffer, C Shan Xu, Michal Januszewski, Zhiyuan Lu, Shin-ya Takemura, Kenneth J Hayworth, Gary B Huang, Kazunori Shinomiya, Jeremy Maitlin-Shepard, Stuart Berg, et al. A connectome and analysis of the adult drosophila central brain. *Elife*, 9: e57443, 2020.

[52] Michael Winding, Benjamin D Pedigo, Christopher L Barnes, Heather G Patsolic, Youngser Park, Tom Kazimiers, Akira Fushiki, Ingrid V Andrade, Avinash Khandelwal, Javier Valdes-Aleman, et al. The connectome of an insect brain. *Science*, 379(6636):eadd9330, 2023.

[53] Olaf Sporns. Structure and function of complex brain networks. *Dialogues in clinical neuroscience*, 15(3): 247–262, 2013.

[54] Azadeh Nematzadeh, Emilio Ferrara, Alessandro Flammini, and Yong-Yeol Ahn. Optimal network modularity for information diffusion. *Physical review letters*, 113(8):088701, 2014.

[55] Edsger W Dijkstra. A note on two problems in connexion with graphs. In *Edsger Wybe Dijkstra: his life, work, and legacy*, pages 287–290. 2022.

[56] Tiago P Peixoto. Hierarchical block structures and high-resolution model selection in large networks. *Physical Review X*, 4(1):011047, 2014.

[57] Richard Betzel, Maria Grazia Puxeddu, and Caio Seguin. Hierarchical communities in the larval drosophila connectome: Links to cellular annotations and network topology. *Proceedings of the National Academy of Sciences*, 121(38):e2320177121, 2024.

[58] Ketan Mehta, Rebecca F Goldin, and Giorgio A Ascoli. Circuit analysis of the drosophila brain using connectivity-based neuronal classification reveals organization of key communication pathways. *Network Neuroscience*, 7(1):269–298, 2023.

[59] Alexander B Kunin, Jiahao Guo, Kevin E Bassler, Xaq Pitkow, and Krešimir Josić. Hierarchical modular structure of the drosophila connectome. *Journal of Neuroscience*, 43(37):6384–6400, 2023.

[60] Leandro González-Montesino, Darian H Grass-Boada, and Rubén Armañnazas. Network community detection in connectomics data using graph theory. In *2023 IEEE International Conference on Bioinformatics and Biomedicine (BIBM)*, pages 3459–3465. IEEE, 2023.

[61] Han SJ Cheong, Igor Siwanowicz, and Gwyneth M Card. Multi-regional circuits underlying visually guided decision-making in drosophila. *Current Opinion in Neurobiology*, 65:77–87, 2020.

[62] Brad K Hulse, Hannah Haberkern, Romain Franconville, Daniel B Turner-Evans, Shin-ya Takemura, Tanya Wolff, Marcella Noorman, Marisa Dreher, Chuntao Dan, Ruchi Parekh, et al. A connectome of the drosophila central complex reveals network motifs suitable for flexible navigation and context-dependent action selection. *Elife*, 10, 2021.

[63] Tomoko Ohyama, Casey M Schneider-Mizell, Richard D Fetter, Javier Valdes Aleman, Romain Franconville, Marta Rivera-Alba, Brett D Mensh, Kristin M Branson, Julie H Simpson, James W Truman, et al. A multilevel multimodal circuit enhances action selection in drosophila. *Nature*, 520(7549): 633–639, 2015.

[64] Dean A Pospisil, Max J Aragon, Sven Dorkenwald, Arie Matsliah, Amy R Sterling, Philipp Schlegel, Szichieh Yu, Claire E McKellar, Marta Costa, Katharina Eichler, et al. The fly connectome reveals a path to the effectome. *Nature*, 634(8032):201–209, 2024.

[65] Christopher J Honey, Rolf Kötter, Michael Breakspear, and Olaf Sporns. Network structure of cerebral cortex shapes functional connectivity on multiple time scales. *Proceedings of the National Academy of Sciences*, 104(24):10240–10245, 2007.

[66] Rubén Herzog, Pedro AM Mediano, Fernando E Rosas, Andrea I Luppi, Yonatan Sanz Perl, Enzo Tagliazucchi, Morten L Kringelbach, Rodrigo Cofré, and Gustavo Deco. Neural mass modelling for the masses: Democratising access to whole-brain biophysical modelling with fastdmf. *Network Neuroscience*, pages 1–38, 2024.

[67] Henry Markram, Eilif Muller, Srikanth Ramaswamy, Michael W Reimann, Marwan Abdellah, Carlos Aguado Sanchez, Anastasia Ailamaki, Lidia Alonso-Nanclares, Nicolas Antille, Selim Arsever, et al. Reconstruction and simulation of neocortical microcircuitry. *Cell*, 163(2):456–492, 2015.

[68] Philipp Schlegel, Alexander Shakeel Bates, Tomke Stürner, Sridhar R Jagannathan, Nikolas Drummond, Joseph Hsu, Laia Serratosa Capdevila, Alexandre Javier, Elizabeth C Marin, Asa Barth-Maron, et al. Information flow, cell types and stereotypy in a full olfactory connectome. *Elife*, 10:e66018, 2021.

[69] Dylan F Cooke and Michael SA Graziano. Sensorimotor integration in the precentral gyrus: polysensory neurons and defensive movements. *Journal of neurophysiology*, 91(4):1648–1660, 2004.

[70] Soo Min Oh, Kyunghwa Jeong, Jeong Taeg Seo, and Seok Jun Moon. Multisensory interactions regulate feeding behavior in drosophila. *Proceedings of the National Academy of Sciences*, 118(7):e2004523118, 2021.

[71] Timothy A Currier and Katherine I Nagel. Multisensory control of navigation in the fruit fly. *Current opinion in neurobiology*, 64:10–16, 2020.

[72] Stefano Boccaletti, Vito Latora, Yamir Moreno, Martin Chavez, and D-U Hwang. Complex networks: Structure and dynamics. *Physics reports*, 424(4-5): 175–308, 2006.

[73] Xiao-Jing Wang and Henry Kennedy. Brain structure and dynamics across scales: in search of rules. *Current opinion in neurobiology*, 37:92–98, 2016.

[74] Christopher W Lynn and Danielle S Bassett. The physics of brain network structure, function and control. *Nature Reviews Physics*, 1(5):318–332, 2019.

[75] Olaf Sporns and Giulio Tononi. Structural determinants of functional brain dynamics. In *Handbook of brain connectivity*, pages 117–147. Springer, 2007.

[76] Olaf Sporns, Giulio Tononi, and Gerald M Edelman. Connectivity and complexity: the relationship between neuroanatomy and brain dynamics. *Neural networks*, 13(8-9):909–922, 2000.

[77] Panagiotis Fotiadis, Linden Parkes, Kathryn A Davis, Theodore D Satterthwaite, Russell T Shinohara, and Dani S Bassett. Structure–function coupling in macroscale human brain networks. *Nature Reviews Neuroscience*, 25(10):688–704, 2024.

[78] Laura E Suárez, Ross D Markello, Richard F Betzel, and Bratislav Misic. Linking structure and function in macroscale brain networks. *Trends in Cognitive Sciences*, 2020.

[79] Kevin Mann, Stephane Deny, Surya Ganguli, and Thomas R Clandinin. Coupling of activity, metabolism and behaviour across the drosophila brain. *Nature*, 593(7858):244–248, 2021.

[80] Xiaoyu Zhang, Pengcheng Yang, Jiawei Feng, Qiang Luo, Wei Lin, and Xin Lu. Simple network mechanism leads to quasi-real brain activation patterns with drosophila connectome. *arXiv preprint arXiv:2404.17128*, 2024.

[81] Nils Eckstein, Alexander Shakeel Bates, Andrew Champion, Michelle Du, Yijie Yin, Philipp Schlegel, Alicia Kun-Yang Lu, Thomson Rymer, Samantha Finley-May, Tyler Paterson, et al. Neurotransmitter classification from electron microscopy images at synaptic sites in drosophila melanogaster. *Cell*, 187 (10):2574–2594, 2024.

[82] Anthony Azevedo, Ellen Lesser, Jasper S Phelps, Brandon Mark, Leila Elabbady, Sumiya Kuroda, Anne Sustar, Anthony Moussa, Avinash Khandelwal, Chris J Dallmann, et al. Connectomic reconstruction of a female drosophila ventral nerve cord. *Nature*, 631 (8020):360–368, 2024.

[83] Roman Vaxenburg, Igor Siwanowicz, Josh Merel, Alice A Robie, Carmen Morrow, Guido Novati, Zinovia Stefanidi, Gwyneth M Card, Michael B Reiser, Matthew M Botvinick, et al. Whole-body simulation of realistic fruit fly locomotion with deep reinforcement learning. *bioRxiv*, pages 2024–03, 2024.

[84] Ellen Lesser, Anthony W Azevedo, Jasper S Phelps, Leila Elabbady, Andrew Cook, Durafshan Sakeena Syed, Brandon Mark, Sumiya Kuroda, Anne Sustar, Anthony Moussa, et al. Synaptic architecture of leg and wing premotor control networks in drosophila. *Nature*, 631(8020):369–377, 2024.

[85] Justine Y Hansen, Simone Cauzzo, Kavita Singh, María Guadalupe García-Gomar, James M Shine, Marta Bianciardi, and Bratislav Misic. Integrating brainstem and cortical functional architectures. *Nature Neuroscience*, pages 1–12, 2024.

[86] Javier Gonzalez-Castillo, Isabel Fernandez, Daniel Handwerker, and Peter Bandettini. Contribution of ultra-slow fmri fluctuations in the 4th ventricle to our understanding of sleep. *bioRxiv*, 2022.

[87] Evelyn MR Lake, Xinxin Ge, Xilin Shen, Peter Herman, Fahmeed Hyder, Jessica A Cardin, Michael J Higley, Dustin Scheinost, Xenophon Papademetris, Michael C Crair, et al. Simultaneous cortex-wide fluorescence ca 2+ imaging and whole-brain fmri. *Nature Methods*, 17(12):1262–1271, 2020.

[88] Elisabeth Ragone, Jacob Tanner, Youngheun Jo, Farnaz Zamani Esfahlani, Joshua Faskowitz, Maria Pope, Ludovico Coletta, Alessandro Gozzi, and Richard Betzel. Modular subgraphs in large-scale connectomes underpin spontaneous co-fluctuation" events" in mouse and human brains. *bioRxiv*, pages 2023–05, 2023.

[89] Richard Betzel and Petra Vértes. Organizing principles of the c. elegans contactome. *Cell Systems*, 12(7): 689–691, 2021.

[90] Olaf Sporns and Jonathan D Zwi. The small world of the cerebral cortex. *Neuroinformatics*, 2(2):145–162, 2004.

[91] Danielle Smith Bassett and ED Bullmore. Small-world brain networks. *The neuroscientist*, 12(6):512–523, 2006.

[92] Martijn P Van Den Heuvel and Olaf Sporns. Rich-club organization of the human connectome. *Journal of Neuroscience*, 31(44):15775–15786, 2011.

[93] Olaf Sporns and Richard F Betzel. Modular brain networks. *Annual review of psychology*, 67:613–640, 2016.

[94] David Meunier, Renaud Lambiotte, and Edward T Bullmore. Modular and hierarchically modular organization of brain networks. *Frontiers in neuroscience*, 4:200, 2010.

[95] Jonathan D Power, Alexander L Cohen, Steven M Nelson, Gagan S Wig, Kelly Anne Barnes, Jessica A Church, Alecia C Vogel, Timothy O Laumann, Fran M Miezin, Bradley L Schlaggar, et al. Functional network organization of the human brain. *Neuron*, 72(4):665–678, 2011.

[96] Jennifer Stiso and Danielle S Bassett. Spatial embedding imposes constraints on neuronal network architectures. *Trends in cognitive sciences*, 22(12):1127–1142, 2018.

[97] Mária Ercsey-Ravasz, Nikola T Markov, Camille Lamy, David C Van Essen, Kenneth Knoblauch, Zoltán Toroczkai, and Henry Kennedy. A predictive network model of cerebral cortical connectivity based on a distance rule. *Neuron*, 80(1):184–197, 2013.

[98] Anastasiya Salova and István A Kovács. Combined topological and spatial constraints are required to capture the structure of neural connectomes. *arXiv preprint arXiv:2405.06110*, 2024.

[99] Jakob Troidl, Simon Warchol, Jinhan Choi, Jordan Matelsky, Nagaraju Dhanyasi, Xueying Wang, Brock

Wester, Donglai Wei, Jeff W Lichtman, Hanspeter Pfister, et al. Vimo-visual analysis of neuronal connectivity motifs. *IEEE transactions on visualization and computer graphics*, 2023.

[100] Jordan K Matelsky, Michael S Robinette, Brock Wester, William R Gray-Roncal, Erik C Johnson, and Elizabeth P Reilly. Data-driven motif discovery in biological neural networks. *bioRxiv*, pages 2023–10, 2023.

[101] Zhihao Zheng, J Scott Lauritzen, Eric Perlman, Camenzind G Robinson, Matthew Nichols, Daniel Milkie, Omar Torrens, John Price, Corey B Fisher, Nadiya Sharifi, et al. A complete electron microscopy volume of the brain of adult drosophila melanogaster. *Cell*, 174(3):730–743, 2018.

[102] Julia Buhmann, Arlo Sheridan, Caroline Malin-Mayor, Philipp Schlegel, Stephan Gerhard, Tom Kazimiers, Renate Krause, Tri M Nguyen, Larissa Heinrich, Wei-Chung Allen Lee, et al. Automatic detection of synaptic partners in a whole-brain drosophila electron microscopy data set. *Nature methods*, 18(7):771–774, 2021.

[103] Larissa Heinrich, Jan Funke, Constantin Pape, Juan Nunez-Iglesias, and Stephan Saalfeld. Synaptic cleft segmentation in non-isotropic volume electron microscopy of the complete drosophila brain. In *Medical Image Computing and Computer Assisted Intervention–MICCAI 2018: 21st International Conference, Granada, Spain, September 16-20, 2018, Proceedings, Part II 11*, pages 317–325. Springer, 2018.

[104] Arie Matsliah, Szi-Chieh Yu, Krzysztof Kruk, Doug Bland, Austin T Burke, Jay Gager, James Hebditch, Ben Silverman, Kyle Patrick Willie, Ryan Willie, et al. Neuronal parts list and wiring diagram for a visual system. *Nature*, 634(8032):166–180, 2024.

[105] Wei-Chung Allen Lee, Vincent Bonin, Michael Reed, Brett J Graham, Greg Hood, Katie Glattfelder, and R Clay Reid. Anatomy and function of an excitatory network in the visual cortex. *Nature*, 532(7599):370–374, 2016.

[106] Richard F Betzel, Katherine C Wood, Christopher Angeloni, Maria Neimark Geffen, and Danielle S Bassett. Stability of spontaneous, correlated activity in mouse auditory cortex. *PLoS computational biology*, 15(12): e1007360, 2019.

[107] Richard F Betzel. Organizing principles of whole-brain functional connectivity in zebrafish larvae. *Network Neuroscience*, 4(1):234–256, 2020.

[108] Travis A Jarrell, Yi Wang, Adam E Bloniarz, Christopher A Brittin, Meng Xu, J Nichol Thomson, Donna G Albertson, David H Hall, and Scott W Emmons. The connectome of a decision-making neural network. *science*, 337(6093):437–444, 2012.

[109] Dragana M Pavlovic, Petra E Vértes, Edward T Bullmore, William R Schafer, and Thomas E Nichols. Stochastic blockmodeling of the modules and core of the caenorhabditis elegans connectome. *PloS one*, 9 (7):e97584, 2014.

[110] Daiki Kiyooka, Ikumi Oomoto, Jun Kitazono, Midori Kobayashi, Chie Matsubara, Kenta Kobayashi, Masanori Murayama, and Masafumi Oizumi. Single-cell resolution functional networks during sleep are segregated into spatially intermixed modules. *bioRxiv*, pages 2023–09, 2023.

[111] Santo Fortunato. Community detection in graphs. *Physics reports*, 486(3-5):75–174, 2010.

[112] Mark EJ Newman and Michelle Girvan. Finding and evaluating community structure in networks. *Physical review E*, 69(2):026113, 2004.

[113] Martin Rosvall and Carl T Bergstrom. Maps of random walks on complex networks reveal community structure. *Proceedings of the National Academy of Sciences*, 105(4):1118–1123, 2008.

[114] Pan Zhang and Cristopher Moore. Scalable detection of statistically significant communities and hierarchies, using message passing for modularity. *Proceedings of the National Academy of Sciences*, 111(51): 18144–18149, 2014.

[115] Gergely Palla, Imre Derényi, Illés Farkas, and Tamás Vicsek. Uncovering the overlapping community structure of complex networks in nature and society. *nature*, 435(7043):814–818, 2005.

[116] Sadamori Kojaku, Filippo Radicchi, Yong-Yeol Ahn, and Santo Fortunato. Network community detection via neural embeddings. *Nature Communications*, 15 (1):9446, 2024.

[117] Carey E Priebe, Youngser Park, Joshua T Vogelstein, John M Conroy, Vince Lyzinski, Minh Tang, Avanti Athreya, Joshua Cape, and Eric Bridgeford. On a two-truths phenomenon in spectral graph clustering. *Proceedings of the National Academy of Sciences*, 116 (13):5995–6000, 2019.

[118] Brian Karrer and Mark EJ Newman. Stochastic blockmodels and community structure in networks. *Physical review E*, 83(1):016107, 2011.

[119] Paul W Holland, Kathryn Blackmond Laskey, and Samuel Leinhardt. Stochastic blockmodels: First steps. *Social networks*, 5(2):109–137, 1983.

[120] Carolyn J Anderson, Stanley Wasserman, and Katherine Faust. Building stochastic blockmodels. *Social networks*, 14(1-2):137–161, 1992.

[121] Tom AB Snijders and Krzysztof Nowicki. Estimation and prediction for stochastic blockmodels for graphs with latent block structure. *Journal of classification*, 14(1):75–100, 1997.

[122] Krzysztof Nowicki and Tom A B Snijders. Estimation and prediction for stochastic blockstructures. *Journal of the American statistical association*, 96(455):1077–1087, 2001.

[123] Leto Peel, Daniel B Larremore, and Aaron Clauset. The ground truth about metadata and community detection in networks. *Science advances*, 3(5):e1602548, 2017.

[124] Richard F Betzel, Maxwell A Bertolero, and Danielle S Bassett. Non-assortative community structure in resting and task-evoked functional brain networks. *bioRxiv*, page 355016, 2018.

[125] Joshua Faskowitz, Xiaoran Yan, Xi-Nian Zuo, and Olaf Sporns. Weighted stochastic block models of the human connectome across the life span. *Scientific reports*, 8(1):1–16, 2018.

[126] Christopher Aicher, Abigail Z Jacobs, and Aaron Clauset. Adapting the stochastic block model to edge-

weighted networks. *arXiv preprint arXiv:1305.5782*, 2013.

[127] Marcus E Raichle. The brain's default mode network. *Annual review of neuroscience*, 38:433–447, 2015.

[128] Tiago P Peixoto. Entropy of stochastic blockmodel ensembles. *Physical Review E*, 85(5):056122, 2012.

[129] Tiago P Peixoto. Efficient monte carlo and greedy heuristic for the inference of stochastic block models. *Physical Review E*, 89(1):012804, 2014.

[130] Tiago P Peixoto. Merge-split markov chain monte carlo for community detection. *Physical Review E*, 102 (1):012305, 2020.

[131] Andrea Lancichinetti and Santo Fortunato. Consensus clustering in complex networks. *Scientific reports*, 2 (1):1–7, 2012.

[132] Tiago P Peixoto. Revealing consensus and dissensus between network partitions. *Physical Review X*, 11(2): 021003, 2021.

[133] J MacQueen. Some methods for classification and analysis of multivariate observations. In *Proceedings of 5-th Berkeley Symposium on Mathematical Statistics and Probability/University of California Press*, 1967.

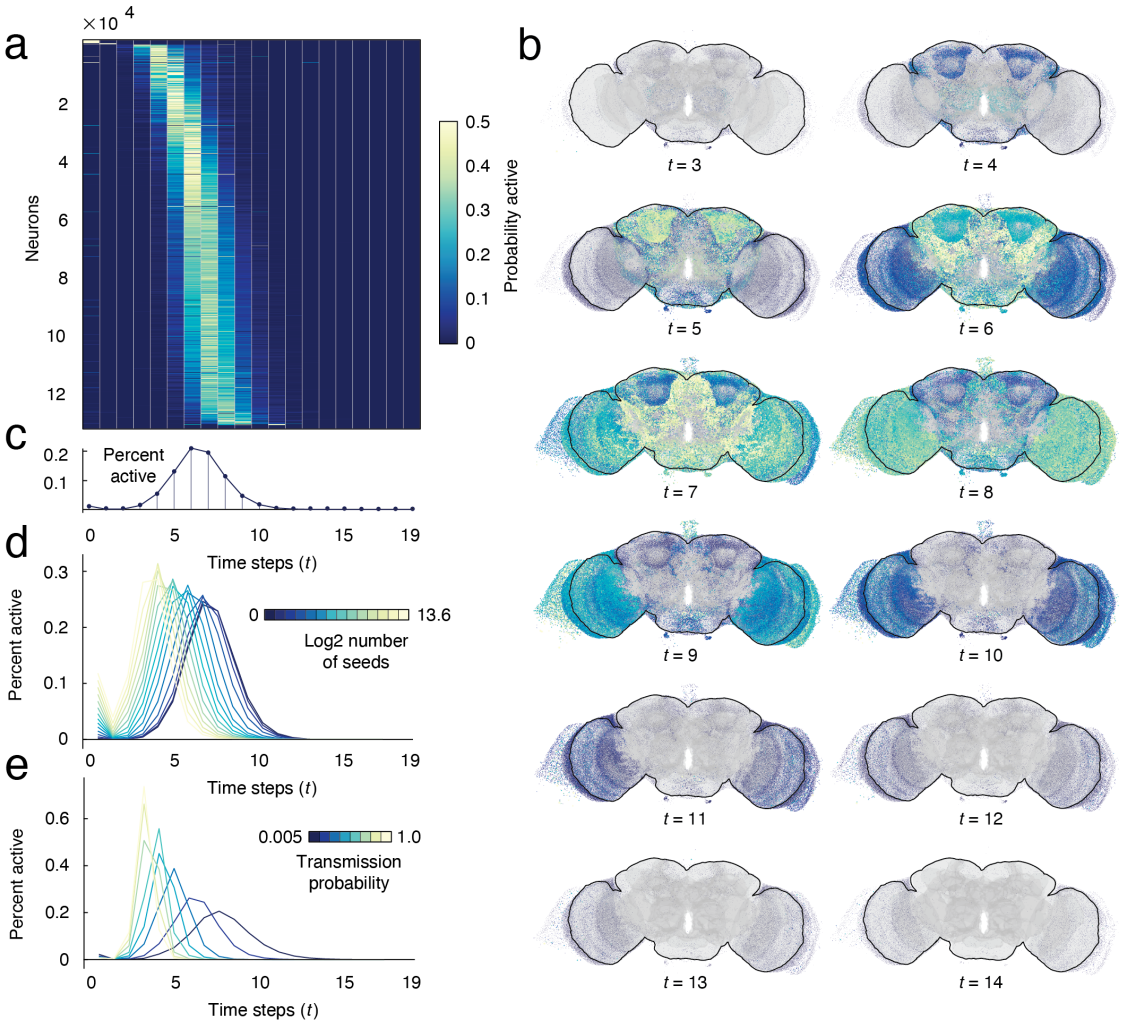

Figure S1. **Unimodal cascades.** We initialize cascades by "seeding" sensory systems with a subset of active neurons. These neurons probabilistically activate their post-synaptic neighbors. (a) Activation probability for all neurons $\times$ time. In this example all sensory neurons were active at time $t = 0$. (b) Percent of neurons active at each time step. (c) Activation probability of each neuron in anatomical space. Note that here we only plot each neuron's soma and omit their arborization. The cascade model depends on two parameters: the number of seed neurons (those active at time $t = 0$) and the probability of transmission *via* a single synapse. Panels d and e illustrate how variation of these parameters impact transmission probability curves. (d) Increasing the number of seed neurons largely shifts the curve to the left. In this example transmission probability was held constant at $p_{transmission} = 0.01$. (e) Increasing transmission probability compresses and shifts and the curve.

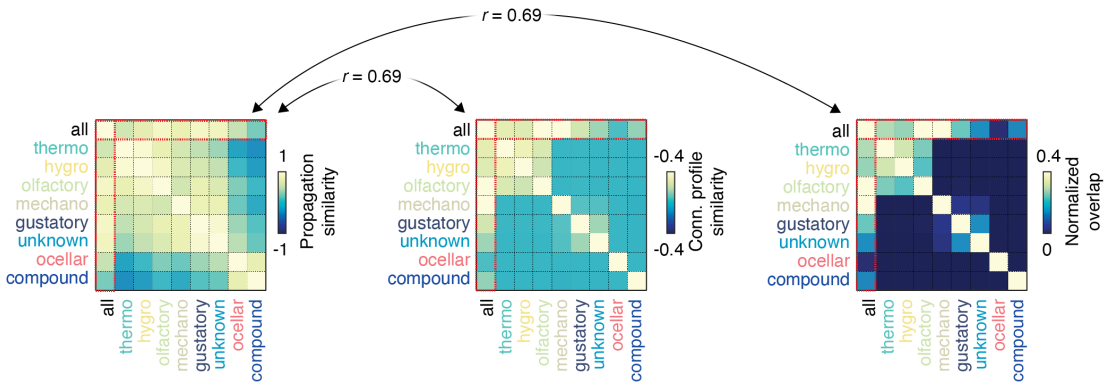

Figure S2. **Cascade similarity *versus* connectivity similarity.** Here, we show cascade similarity (from Fig. 4) alongside the similarity of connectivity profiles. Specifically, we calculated the an average connectivity profile (outgoing connections only) for all each sensory modalities combined (all) and for each sensory modality independently. The center plot shows correlations between profiles; the right plot shows normalized dot product.

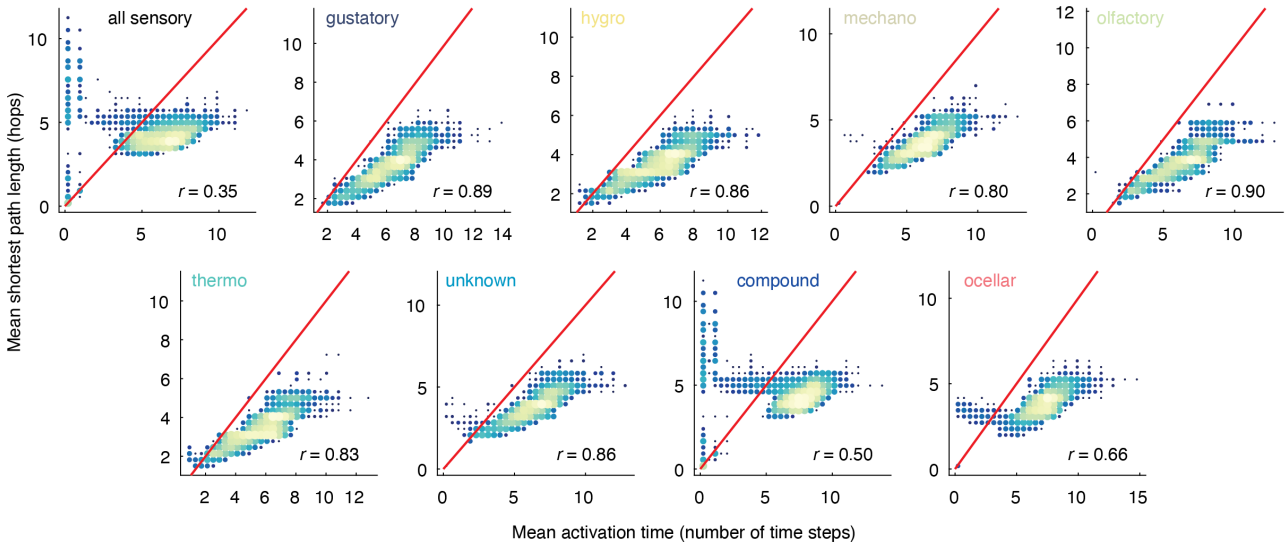

Figure S3. **Comparing shortest paths with activation times.** In the main text we reported activation times of neurons given different sensory seeds. To verify that these activation times were not strictly the consequence of shortest paths, we calculated the binary shortest path from each neuron to all other neurons in the network. For a given sensory modality, we calculated the average distance of all such sensory neurons to all other neurons in the *Drosophila* brain. We then compared those distances (measured in number of hops) with activation times. The above figures show mean activation times plotted as a function of mean shortest path for all eight sensory modalities as well as all sensory modalities combined. Note that size and color intensity of markers in each plot are proportional to the log density.

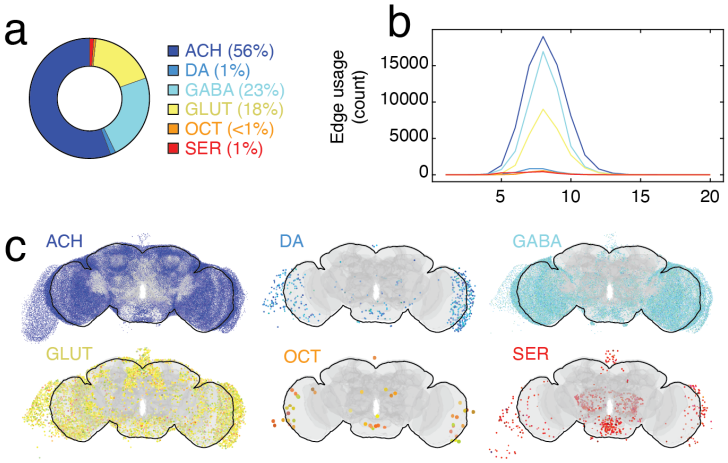

Figure S4. **Effect of synapse type on activation time.** In the main text we grouped all synapses together, making no distinction between neurotransmitter types. Here, we parse contributions made by six distinct synapse types (based on neurotransmitter). They include acetylcholine (ACH), dopamine (DA), gabaergic (GABA), glutamate (GLUT), octopamine (OCT), and seratonin (SER). (*a*) Percent of all synapses associated with each neurotransmitter. (*b*) We tracked how frequently synapses associated with different neurotransmitter types successfully activated their post-synaptic partner. In this plot, we show edge usage (number of active synapses of each type) as a function of time steps. Note that this plot was generated as the mean usage over 1000 simulations with all sensory modalities included in the seed set but with seed size fixed at 16 with transmission probability of $p_{tranmission} = 0.01$. (*c*) For each neuron, we calculated when it was first activated by by what neurotransmitter. This plot depicts, as a function of neurotransmitter, neurons likely to be activated by each of the six neurotransmitters.

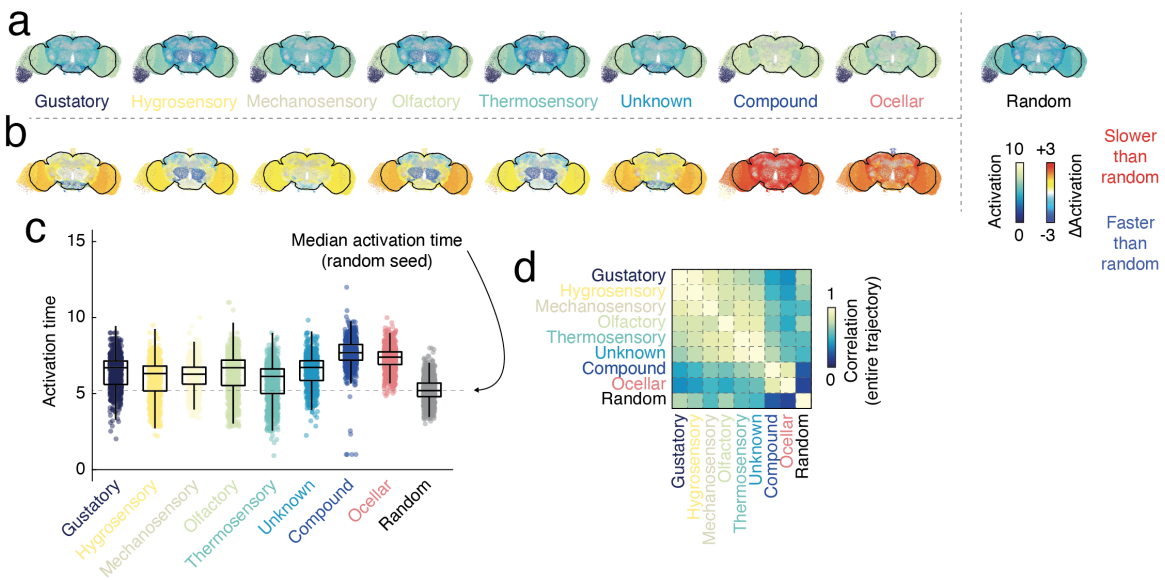

Figure S5. **Comparing random and sensory seeds.** (*a*) Mean activation time for neurons for eight sensory modalities. To the far right we show activation time for the random map. (*b*) Difference between random and sensory cascades in terms of activation time. (*c*) Boxplot of differences. (*d*) Correlation of entire (vectorized and concatenated) trajectory.

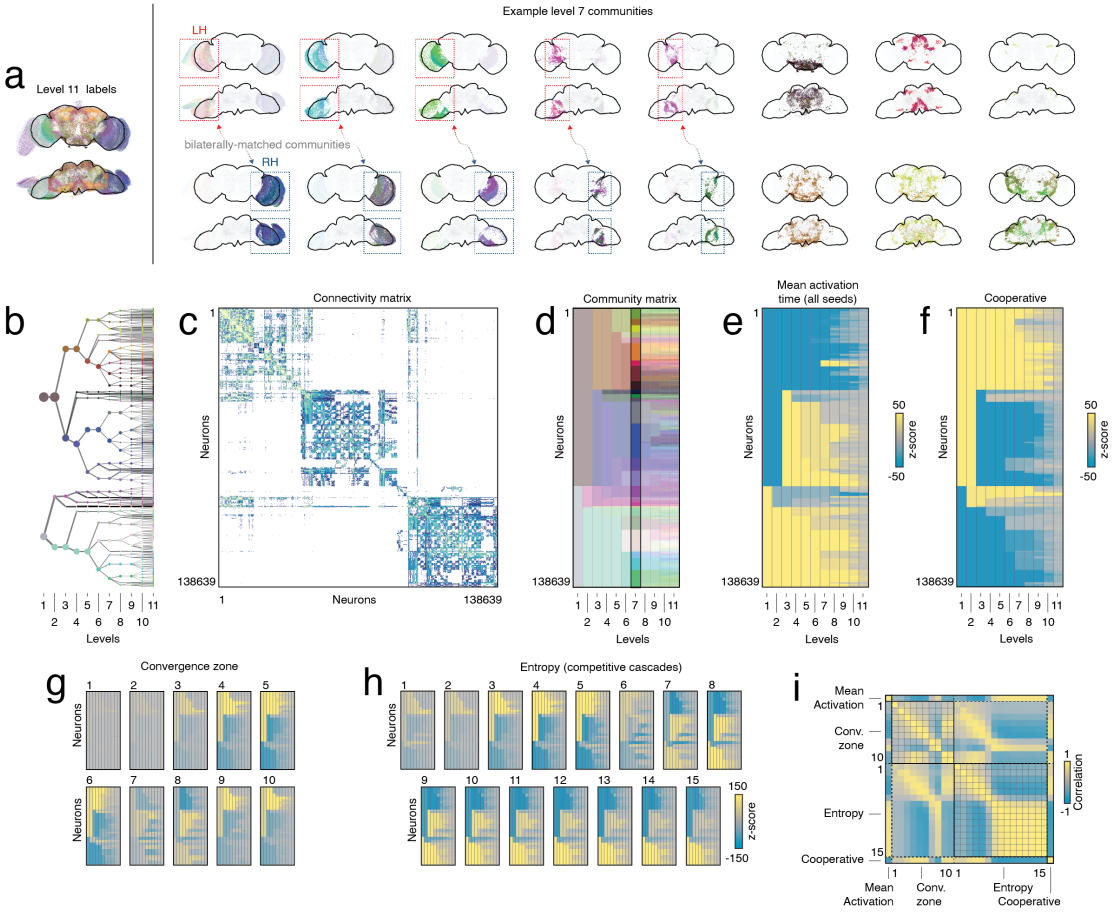

Figure S6. **Linking the modular structure of the connectome with cascade statistics.** We used a hierarchical community detection algorithm to divide neurons into nested blocks. (*a*) Topography of all communities with their finest (level 11) coloration. To the right, we show example communities from an intermediate scale (level 7). We highlight pairs of communities that are lateralized as well as their partners in the opposite hemisphere. (*b*) Community dendrogram. (*c*) Connectivity matrix ordered by communities. (*d*) An alternative visualization of community labels; each column is hierarchical level with rows ordered by communities. The colors of entries correspond to community labels. Panels *e*-*h* show enrichment scores for communities at all hierarchical levels for: (*e*) Mean activation time; (*f*) Average reduction in activation time during cooperative cascades; (*g*) Convergence zone as a function of time step (from $t = 1$ to $t = 10$), and (*h*) Entropy during competitive cascades (from $t = 1$ to $t = 15$). (*i*) For each measure (and each time step, for those that were temporally resolved), we retained for each community its enrichment score. We represented these scores as vectors and computed the correlation between all such vectors to yield a similarity matrix. The "hot" elements of the matrix identified enrichment patterns that were highly similar; "cooler" elements correspond to dissimilar and anti-correlated enrichment patterns.

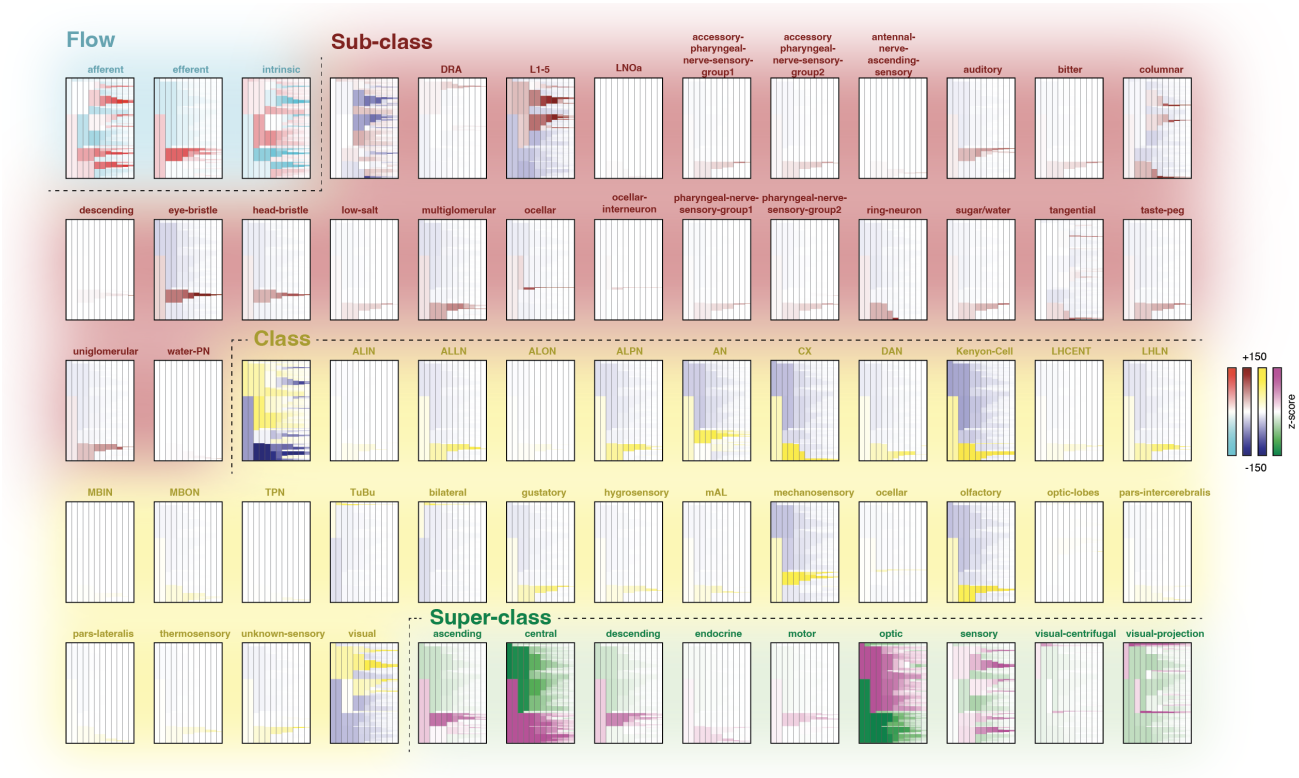

Figure S7. **Enrichment analysis of community labels within annotation data.** Each plot corresponds to a specific annotation. Each plot shows annotation enrichment across 11 hierarchical levels of communities. The colormap differs across annotations based on annotation category (Flow, sub-class, class, and super-class). Hot colors correspond to communities significantly enriched for an annotation; cooler colors correspond to communities that are avoidant with respect to a given annotation.

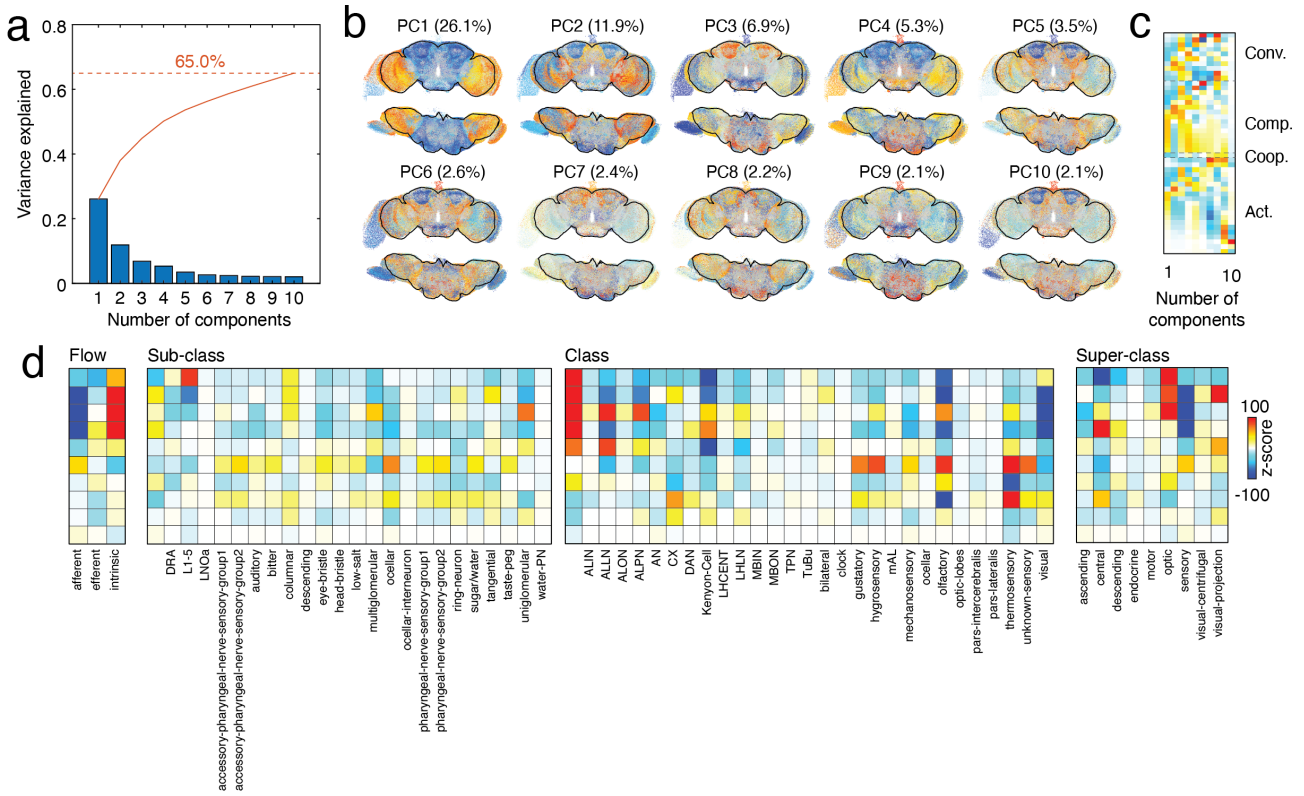

Figure S8. **Principal component analysis of cascade statistics.** In the main text, we clustered neurons to identify groups with similar cascade statistics–i.e. convergence, speed-ups, entropy, and activation times. Here, we apply PCA to the same data (after z-scoring columns). (*a*) Variance explained by each of the first 10 components (in blue). Cumulative variance explained shown in orange. (*b*) Spatial maps (components). (*c*) Coefficients. (*d*) Enrichment of spatial maps across annotations.